Modelling of organic Rankine cycle efficiency with respect to the equivalent hot side temperature

Jing Li[1], Jahan Zeb[1] Alvi, Gang Pei[1]*, Yuehong Su[2], Pengcheng Li[1], Guangtao Gao[1], Jie Ji[1]

[1]Department of Thermal Science and Energy Engineering, University of Science and Technology of China, 96 Jinzhai Road ,Hefei, China

[2]Institute of Sustainable Energy Technology, University of Nottingham, University Park, Nottingham NG7 2RD, UK

Abstract: An indicator, namely equivalent hot side temperature (T_{EHST}) is proposed for the organic Rankine cycle (ORC). T_{EHST} is derived from ideal thermodynamic process, but can denote the efficiency of irreversible ORC. Study on 27 fluids shows that given the operating conditions, fluid of higher T_{EHST} generally offers higher ORC efficiency. This relationship is stronger and more universal than those established with respect to the critical temperature, boiling point temperature, Jacobs number and Figure of Merit. An ORC model by the method of error transfer and compensation is further built, in which the efficiency is quantitatively correlated with T_{EHST}. Unlike the conventional ORC efficiency model, this one consists of thermodynamic parameters on the liquid/vapor curve and is independent on fluid properties at superheated state, and hence is more convenient. It has high accuracy especially for basic ORC and the relative deviation of the estimated efficiency from that calculated by the conventional model is from -0.7% to 3.4 %. The novel model is applied for the thermodynamic performance prediction of a recently developed fluid of HFO1336mzzZ based on the phase equilibrium data. The results indicate HFO1336mzzZ is more efficient than R245fa on the conditions of high evaporation temperature and low

pump efficiency.

Keywords: *organic Rankine cycle; equivalent hot side temperature; efficiency indicator; liquid-vapor equilibrium; error*

*Corresponding author. Tel./Fax: +86 551 63607367. E-mail: peigang@ustc.edu.cn.

1. Introduction

Organic Rankine cycle (ORC) has been proven to be one of the most promising and efficient technologies for converting low-grade heat e.g. solar thermal energy, geothermal energy, industrial waste heat, biomass energy and ocean thermal energy into electricity[1, 2]. In the past decade, effect of working fluid on the performance of the ORC system has been studied intensively. Different indicators have been proposed such as vapor density, liquid specific heat, molecular entropy, enthalpy ratio, boiling point temperature, critical temperature, Jacobs number and Figure of Merit (FOM). These indicators are good guidelines for the ORC performance assessment.

Low vapor density is accompanied by high volume flow rate which leads to large pressure drop across the heat exchanger. The size of the expander must be also increased which significantly affects the cost of the system [3, 4]. Low liquid specific heat of the working fluid can decrease work done by the pump and increase work output indirectly [3, 5, 6]. For subcritical ORC systems, fluids having lower molecular entropies result in higher thermal efficiencies [7]. The effect of the boiling point temperature of working fluids on the ORC performance has been investigated, and higher boiling point temperature causes higher evaporation pressure [8]. Enthalpy ratio (ratio of the latent heat of vaporization to the sensible heat) strongly influences the energetic and exergetic efficiency of ORC system.

Higher enthalpy ratio elevates the amount of heat during phase change process. Hence, higher ORC efficiency is achieved while avoiding superheat and regeneration [9].

Jacobs number has been proposed [10], which is correlated to the latent and sensible heat.

$$Ja = C_p dT / Hv \tag{1}$$

where $C_p dT$ is the sensible heat and Hv is the vaporization latent heat. Thermal efficiency of the ORC system decreases with the increment in Jacobs number. A dimensionless FOM combining Jacobs number, evaporation temperature and condensation temperature has been further put forward by Kuo et al [11]. Similarly, thermal efficiency decreases with the increment in FOM.

$$Figure\ of\ Merit = Ja^{0.1}(\frac{T_{cond}}{T_{evp}}) \tag{2}$$

Among the properties of the working fluid, the critical temperature is one of the most relevant indicators that affect the thermodynamic performance of ORC. The influence of fluid critical temperature on the efficiencies of isolated ORC [8, 12, 13], geothermal ORC [14], waste heat recovery [8, 15, 16] and solar ORC [3] has been evaluated by lots of researchers. More efficient power conversion can be facilitated by using fluid of higher critical temperature. This conclusion is applicable for most working fluids.

Besides, extensive investigation has been performed on the resultant role of working fluid properties in the net power output [17-19], ratio of power output to heat exchanger area [20, 21], net output per unit mass flow rate [22], installation cost per net power output [23-27], exergy efficiency [28-32] and overall system performance [33-35].

The aforementioned indicators are linked with the ORC behavior. They make the working fluid selection more commodious. However, the quantitative relationship between the ORC efficiency and these indicators is lacked. In the present study, an equivalent hot side temperature (T_{EHST}) is proposed. It is a new indicator rooted in the fundamental of thermodynamics. The effect of T_{EHST} on the ORC efficiency is examined on various operating conditions. A mathematical model of the ORC efficiency in view of T_{EHST} is further established. This model can overcome some disadvantages of the conventional ORC efficiency model. For the latter, thermodynamic information (enthalpy, entropy, et al.) on expander outlet must be known in order to ascertain the cycle efficiency. The parameters at superheated state are correlated with the fluid PVT (pressure-volume-temperature) behavior. It is a cumbersome process to get accurate PVT behavior in a wide range of temperature and pressure. Many fluids especially newly developed fluids are unavailable in commercial database such as REFPROP and CoolProp. Their ORC efficiencies cannot be predicted in a convenient way using the traditional model. For the novel model, only thermodynamic parameters at liquid-vapor equilibrium state are involved. The enthalpy and entropy at superheated state are dispensable. The deduction, accuracy and applicability of the model are investigated in the following sections.

Twenty-seven dry and isentropic working fluids are selected. For dry fluids, optimum ORC efficiency can be achieved since they operate along the saturation vapor curve without being superheated [36-38]. Similarly, in case of an isentropic fluid a nearly vertical vapor saturation curve can be obtained. Vapor remains saturated till the end of expansion process and there is no need for regeneration [39].

2. Derivation of the equivalent hot side temperature

The *T-s* diagram of ORC is depicted in Fig.1. An ideal ORC cycle (1-2s-3-4s-1) is comprised by four basic processes: (1) isentropic pressurization by the pump; (2) isobaric heating in the evaporator; (3) isentropic expansion through the expander; (4) isobaric cooling in the condenser.

Thermal efficiency of the ideal ORC is expressed by

$$\eta_{t,id} = 1 - \frac{q_{o,id}}{q_{i,id}} \tag{3}$$

The input and output heat are equal to

$$q_{i,id} = \int_{2s}^{3} Tds = h_3 - h_{2s} \tag{4}$$

$$q_{o,id} = \int_{1}^{4s} Tds = h_{4s} - h_1 \tag{5}$$

The equivalent hot side temperature is determined by

$$T_{EHST} = \frac{q_{i,id}}{\Delta s} = \frac{h_3 - h_{2s}}{s_3 - s_{2s}} \tag{6}$$

T_{EHST} has a physical meaning. A higher T_{EHST} represents a stronger force driving the ORC. Analogously, the equivalent cold side temperature is

$$T_{ECST} = \frac{q_{o,id}}{\Delta s} = \frac{h_{4s} - h_1}{s_{4s} - s_1} \tag{7}$$

Therefore, with $S_3 = S_{4s}$ and $S_1 = S_{2s}$, the ORC thermal efficiency can be calculated by

$$\eta_{t,id} = 1 - T_{ECST} / T_{EHST} \tag{8}$$

Most ORC fluids at liquid state are not compressible and most of the heat is taken out by the condensation process. Therefore,

$$h_{2s} \approx h_1 + v_1(p_{2s} - p_1) \tag{9}$$

$$T_{ECST} \approx T_1 \tag{10}$$

$$T_{EHST} = \frac{h_3 - h_{2s}}{s_3 - s_{2s}} \approx \frac{h_3 - h_1 - v_1(p_3 - p_1)}{s_3 - s_1} \tag{11}$$

The right side of Eq.(11) consists of specific enthalpy, specific entropy, specific volume and pressure on the saturation liquid/vapor curve. p_3, h_3 and s_3 are pressure, specific enthalpy and entropy of the saturation vapor at T_3, respectively, while s_1, p_1, h_1 and v_1 are the parameters of the saturation liquid at T_1. Given a fluid, T_{EHST} is a function of the evaporation temperature (T_3) and condensation temperature (T_1). T_1 is generally subject to the environment temperature and ranges from 20 °C to 40 °C, so T_{EHST} is mainly determined by T_3.

It is easy to establish database on T_{EHST}. A sample is presented in Table 1. T_1 is 30 °C. T_3 varies from 100 °C to 150 °C. The fluids are listed in sequence of critical temperature. Benzene has the highest critical temperature of 288.9 °C, while R227ea has the lowest one of 101.7 °C. Only subcritical ORC is considered. With T_{EHST}, the ORC efficiency can be estimated as shown below.

3. New models for the ORC

3.1. Irreversible ORC efficiency with respect to T_{EHST}

A practical ORC (1-2-3-4-1) regarding the thermodynamic irreversibility in the expander, pump and generator has the thermal efficiency as expressed by

$$\eta_t = \frac{w_{e,id} . \varepsilon_e . \varepsilon_g - w_{p,id} / \varepsilon_p}{q_i} \tag{12}$$

$$w_{e,id} = h_3 - h_{4s} \tag{13}$$

$$w_{p,id} = h_{2s} - h_1 \tag{14}$$

$$q_i = h_3 - h_2 \tag{15}$$

Notably, to obtain the output power in an ideal expansion process, enthalpy at the expander outlet shall be known. In this work, a more convenient equation is developed and the relationship between η_t and T_{EHST} is deduced.

$$\eta_{t,id} = \frac{w_{e,id} - w_{p,id}}{q_{i,id}} = \frac{w_{e,id}(1-a)}{q_{i,id}} \tag{16}$$

where *a* is the ratio of pump power to expander power.

$$a = \frac{w_{p,id}}{w_{e,id}} \tag{17}$$

$h_2 - h_{2s}$ is generally far less than q_i. Therefore,

$$q_i \approx q_{i,id} \tag{18}$$

$$\begin{aligned} \eta_t &= \frac{w_{e,id} . \varepsilon_e . \varepsilon_g - a \cdot w_{e,id} / \varepsilon_p}{q_i} \\ &= \frac{w_{e,id}(\varepsilon_e . \varepsilon_g - a / \varepsilon_p)}{q_i} \\ &\approx \eta_{t,id} \frac{\varepsilon_e . \varepsilon_g - a / \varepsilon_p}{1-a} \end{aligned} \tag{19}$$

The ORC efficiency is achieved by combing Eqs. (8) and (19)

$$\eta_t \approx (1 - \frac{T_{ECST}}{T_{EHST}}) \cdot \frac{\varepsilon_e . \varepsilon_g - a / \varepsilon_p}{1-a} \tag{20}$$

3.2. Ratio of pump power to expander power (*a*-value)

The technical work during an ideal expansion is calculated by

$$w_{e,id} = -\int_3^{4s} v dp \tag{21}$$

The integration path is $L_{3\to 4s}$ as depicted by the dash red line in Fig.1.

Assuming the specific volume of saturated vapor (v_s) at a given pressure of p is approximately equal to v in the ideal expansion process,

$$v_s\Big|_p \approx v\Big|_p \tag{22}$$

A reference expander power is then expressed by

$$w_r = -\int_3^{4'} v_s dp \tag{23}$$

The integration path is $L_{3\to 4'}$ as depicted by the dash blue line in Fig.1. w_r differs from $w_{e,id}$ because v in Eq.(21) is usually larger than v_s in Eq.(23) for each p owing to a degree of superheat along $3 \to 4$s. For example, if $T_{4s}/T_{4'} = 333/303$ then $v_{4s}/v_{4'} \approx 1.1$ based on the ideal gas state equation. Difference between w_r and $w_{e,id}$ exists, and w_r is expected to be lower than $w_{e,id}$. For an approximation,

$$w_{e,id} \approx w_r \tag{24}$$

a can be modelled as

$$a \approx \frac{w_{p,id}}{w_r} \approx \frac{v_1(p_3 - p_1)}{-\int_3^{4'} v_s dp} \tag{25}$$

The relationship $p = f(T)$ between saturation vapor pressure and temperature can be determined by the Antoine Equation (Eq.26) or Wagner Equation (Eq.27) or modified Riedel Equation (Eq.29),

$$\log_{10}(p) = A - \frac{B}{T + C} \tag{26}$$

$$\ln\frac{p}{p_c}=\frac{T_c}{T}(A_1\tau+A_2\tau^{1.5}+A_3\tau^{2.5}+A_4\tau^5) \tag{27}$$

$$\tau=\frac{T_c-T}{T_c} \tag{28}$$

$$\ln p=A'+B'/T+C'\ln T+D'T^2+E'/T^2 \tag{29}$$

The saturation liquid and vapor densities of the HCFO and fluorobutene compounds can be estimated by the scaling law and the law of rectilinear diameters [40, 41].

$$\rho^L-\rho^V=M\tau^\beta \tag{30}$$

$$\rho^L+\rho^V=2(\rho_c+N\tau) \tag{31}$$

By combining Eqs. (26)-(31), $\int_3^{4'} v_s dp$ is achieved.

3.3. New ORC efficiency model by approximating T_{ECST} and *a*-value

With Eqs.(10), (20) and (25), a new ORC efficiency model is built

$$\eta_t\approx(1-\frac{T_1}{T_{EHST}})\cdot\frac{\varepsilon_e.\varepsilon_g+v_1(p_3-p_1)\Big/(\varepsilon_p\int_3^{4'}v_s dp)}{1+v_1(p_3-p_1)\Big/\int_3^{4'}v_s dp} \tag{32}$$

Similarly with T_{EHST} , η_t is comprised of thermodynamic parameters at liquid-vapor equilibrium state.

3.4. Error analysis of the new ORC efficiency model

With the reference of Eqs.(18) and (20), the error in the new ORC efficiency model is mainly caused by the assumptions of $v_s\big|_p\approx v\big|_p$, $T_{ECST}\approx T_1$ and $q_i\approx q_{i,id}$.

3.4.1. Error contributed by the approximation of *a*-value

The derivative of η_t with respect to a is

$$\frac{d\eta_t}{da} \approx (1-\frac{T_{ECST}}{T_{EHST}}) \cdot \frac{\varepsilon_e . \varepsilon_g - 1/\varepsilon_p}{(1-a)^2} \tag{33}$$

Therefore,

$$\frac{\Delta\eta_t}{\eta_t} \approx \frac{\varepsilon_e . \varepsilon_g . \varepsilon_p - 1}{(\varepsilon_e . \varepsilon_g . \varepsilon_p - a)(1-a)} \Delta a \tag{34}$$

With 10% relative error in a, the relative error in η_t is about

$$\frac{\Delta\eta_t}{\eta_t} \approx \frac{\varepsilon_e . \varepsilon_g . \varepsilon_p - 1}{(\varepsilon_e . \varepsilon_g . \varepsilon_p - a)(1-a)} \cdot a \cdot 10\% \tag{35}$$

For most fluids in subcritical ORC, a is less than 0.1. With ε_e, ε_g, ε_p of about 75%, 85% and 65%, $\Delta\eta_t / \eta_t$ is expected to be less than 2%.

Notably, if Eq.(24) is used to approximate the ORC efficiency in the conventional model expressed by Eq.(12), the relative error in η_t will be much larger as follows.

$$\frac{d\eta_t}{dw_{e,id}} = \frac{\varepsilon_e . \varepsilon_g}{q_i} \tag{36}$$

$$\frac{\Delta\eta_t}{\eta_t} \approx \frac{\varepsilon_e . \varepsilon_g}{w_{e,id} . \varepsilon_e . \varepsilon_g - w_{p,id} / \varepsilon_p} \Delta w_{e,id} \tag{37}$$

The error in *a*-value is expected to be similar with that in $w_{e,id}$ according to Eq.(17). With 10% relative error in $w_{e,id}$, the relative error in η_t is about

$$\frac{\Delta\eta_t}{\eta_t} \approx \frac{\varepsilon_e . \varepsilon_g}{\varepsilon_e . \varepsilon_g - \frac{w_{p,id}}{w_{e,id}} \cdot \frac{1}{\varepsilon_p}} 10\% \approx 13\% \tag{38}$$

It is evident that, in light of the approximation of $w_{e,id}$, the ORC efficiency modelled by Eq.(32) is more accurate than that modelled by Eq.(12) due to the error transfer from $w_{e,id}$

to a. In other words, the effect of mis-estimation of $w_{e,id}$ on the ORC efficiency calculated by the conventional model is much more significant than that on the efficiency obtained by the new model.

One reason is that $w_{e,id}$ does not act as an independent variable. It can be determined by Eq.(13). There are different forms of $\eta_{t,id}$ as expressed by Eqs.(3) and (16), in which the partial derivative of $\eta_{t,id}$ with respect to $w_{e,id}$ varies. The derivative is zero for Eq.(3) while it is positive in terms of Eq.(16). Analogically, the partial derivative of η_t with respect to $w_{e,id}$ is different when the form changes from Eq.(12) to Eq.(20).

3.4.2. Error contributed by the approximation of T_{ECST}

For $T_{ECST} \approx T_1$, error exists since most fluids leave the expander at superheated state. The derivative of η_t with respect to T_{ECST} is

$$\frac{d\eta_t}{dT_{ECST}} \approx -\frac{1}{T_{EHST}} \cdot \frac{\varepsilon_e . \varepsilon_g - 1/\varepsilon_p}{1-a} \tag{39}$$

Therefore,

$$\frac{\Delta\eta_t}{\eta_t} \approx -\frac{\Delta T_{ECST}}{T_{EHST} - T_{ECST}} \tag{40}$$

For commercial ORC systems, the temperature difference between the hot and cold sides is generally larger than 80 ºC. Because the latent heat is prominent in the cooling process for most ORC fluids, $T_{ECST} - T_1$ shall be small. Fig.2 shows the variation of T_{ECST} with the degree of superheat ($T_{4s} - T_1$) at the expander outlet on the condition of T_1=30 ºC. $T_{ECST} - T_1$ is less than 1ºC even when the degree of superheat reaches 20 ºC. With an error in $|\Delta T_{ECST}|$ of 1 ºC, $\Delta\eta_t / \eta_t$ is expected to be less than 1.25%. More information on $T_{ECST} - T_1$ is

provided in Table 2. The condensation temperature is 30 °C and the evaporation temperature ranges from 100 °C to 150 °C. Ideal ORC process is assumed. $T_{ECST} - T_1$ is up to 3.29 °C with $\Delta\eta_t / \eta_t$ of about 4.06%.

3.4.3. Error counteraction by the approximation of *a*-value and T_{ECST}

The new ORC model is developed by an error counteraction method. On one hand, the approximation of $T_{ECST} \approx T_1$ will result in a lower cold side temperature and thus a higher ORC efficiency than the real. On the other hand, the approximation of $v_s\big|_p \approx v\big|_p$ will lead to a higher a-value and thus a lower ORC efficiency. The new ORC efficiency model will benefit from the two competitive effects.

The overall error in regard to the approximation of *a*-value and T_{ECST} is expressed by

$$\begin{aligned}(\frac{\Delta\eta_t}{\eta_t})_{over} &\approx (\frac{\Delta\eta_t}{\eta_t})_{ECST} + (\frac{\Delta\eta_t}{\eta_t})_a \\ &\approx -\frac{1}{T_{EHST} - T_{ECST}}\Delta T_{ECST} + \frac{\varepsilon_e.\varepsilon_g.\varepsilon_p - 1}{(\varepsilon_e.\varepsilon_g.\varepsilon_p - a)(1-a)}\Delta a\end{aligned} \tag{41}$$

Because

$$\Delta T_{ECST} < 0$$

$$\Delta a > 0$$

$$T_{ECST} < T_{EHST}$$

$$a < \varepsilon_e.\varepsilon_g.\varepsilon_p < 1$$

$$(\frac{\Delta\eta_t}{\eta_t})_a < 0$$

$$(\frac{\Delta\eta_t}{\eta_t})_{ECST} > 0$$

Therefore, the absolute error shall fulfill

$$\left|(\frac{\Delta\eta_t}{\eta_t})_{over}\right| < \max\{\left|(\frac{\Delta\eta_t}{\eta_t})_{ECST}\right|, \left|(\frac{\Delta\eta_t}{\eta_t})_{a}\right|\} \tag{42}$$

For isentropic fluids, expansion proceeds on the saturation vapor curve, and the errors in a-value and T_{ECST} will be negligible. For dry fluids, a higher degree of superheat after expansion leads to larger difference between T_{ECST} and T_1. Meanwhile, the deviation of $v_s\big|_p$ from $v\big|_p$ gets more significant. The error in ORC efficiency with $T_{ECST} \approx T_1$ can be compensated by $v_s\big|_p \approx v\big|_p$.

3.4.4. Error contributed by the approximation of q_i

Due to the irreversible pumping process, q_i is not equal to $q_{i,id}$. The error in approximating q_i is expressed by

$$\mu(q_i) = \frac{q_{i,id} - q_i}{q_i} \tag{43}$$

Because $q_{i,id}$ is always higher than q_i, the assumption of $q_{i,id} \approx q_i$ will make the estimated efficiency lower than the true value according to Eq.(19). And the relative error in efficiency should be the opposite number of $\mu(q_i)$. Table 3 lists $\mu(q_i)$ on different working conditions. The pump efficiency is assigned to be 50%. The condensation temperature is 30 °C. The maximum $\mu(q_i)$ is 1.78%. In most cases, it is below 1%. Lower $\mu(q_i)$ will be accompanied with more efficient pump. Meanwhile, fluid of greater cycle pressure range in the given temperature interval contributes to a higher pumping power demand [42], and a higher $\mu(q_i)$ generally eventuates.

3.4.5. Deviation of the estimated ORC efficiency

Above all, high accuracy can be expected for the new model and only thermodynamic parameters at liquid-vapor equilibrium state are involved. For a comparison, the deviation of the ORC efficiency modelled by Eq.(32) from that calculated by REFPROP 9.0 using Eq.(12) is defined as

$$\mu(\eta_t) = \frac{\eta_{t,EHST} - \eta_{t,REFP}}{\eta_{t,REFP}} \tag{44}$$

4. Results and discussion

Some assumptions are made while carrying out the simulation: (1) Evaporation and condensation processes are isobaric. (2) Expansion and compression processes are adiabatic. (3) Basic ORC consisting of expander, pump, evaporator and condenser is exemplified.

4.1. Influence of the equivalent hot side temperature on the ORC efficiency under different conditions

In this section influence of T_{EHST} of the working fluids on the ORC cycle efficiency is evaluated on different operating conditions of evaporation and condensation temperatures, and expander and pump efficiencies. Fig.3 shows variation of the ORC efficiency with T_{EHST} at evaporation temperatures of 100^{o}C, 120^{o}C and 150^{o}C, respectively. To avoid crowd in the figure, seventeen working fluids are involved. The condensation temperature is 30 ^{o}C. The expander, pump and generator efficiencies are 75%, 65% and 85%. The ORC efficiency is calculated by Eq. (12) and the thermodynamic parameters are based on REFPROP 9.0. Since this study is focused on subcritical cycle, some of the fluids whose critical temperatures are lower than the evaporation temperature are not selected at 120 ^{o}C and 150^{o}C. Given the evaporation and condensation temperature, there is one-to-one

correspondence between T_{EHST} and the working fluid. ORC efficiency is found to be a strong function of $T_{EHST.}$ It increases almost linearly with the increment in T_{EHST}, which is consistent with the Carnot theory.

Fluids of higher value of T_{EHST} show larger increment in ORC efficiency as compared to fluids of lower T_{EHST} when the evaporation temperature increases. Therefore, ORC efficiency difference between any two fluids increases. For example, at evaporation temperature of 100^{o}C, relative increment in ORC efficiency of benzene over butane is 14.36 % while it is 31.82 % at evaporation temperature of 150^{o}C.

Notably, though the variations of ORC efficiency with T_{EHST} are similar for different evaporation temperatures, the sequences of working fluids are different. For example, cisbutene has higher cycle efficiency than tranbutene at 100 ^{o}C, but when the evaporation temperature is 150 ^{o}C, the opposite is true. The reason is that the efficiency varies in a distinguishable way for each fluid. Some fluids have shown minor increment or even decrement in the ORC efficiency when the evaporation temperature increases, as depicted by the dashed lines in Fig.3. When increasing evaporation temperature from 120^{o}C to 150^{o}C, ORC efficiencies of cisbutene and transbutene increase merely by 0.004 % and 0.93%, respectively. Thanks to T_{EHST}, the efficiency characteristic of each fluid can be explored. Fig.4 shows the variation of the T_{EHST} with the evaporation temperature. R236fa, isobutane, R245fa are taken as examples. T_{EHST} increases with the increment in the evaporation temperature, but not in a monotone way. It decreases when evaporation temperature moves close to the fluid critical temperature. The decrement of T_{EHST} is caused by the significant drop of latent heat (H) as the evaporation temperature (T_3) increases, which can be expressed by the derivative of the function $H=f(T_3)$. At 100 ^{o}C, dH/dT_3 is

about -1.46, -2.4 and -1.0 kJ/ ºC for R236fa, isobutane and R245fa. It becomes -7.4 kJ/K for R236fa at 123 ºC, -18.3 kJ/ ºC for isobutene at 133 ºC and -25.8 kJ/ ºC for R245fa at 153 ºC.

Effect of T_{EHST} of the working fluids on the ORC efficiency at expander efficiency of 65% and 85% is shown in Fig.5. The evaporation temperature and condensation temperature are 100 ºC and 30 ºC. The pump efficiency is 65%. T_{EHST} is independent on the expander efficiency. However, the ORC efficiency decreases with the decrement in the expander efficiency. The efficiency curves are almost parallel. When the expander efficiency increases from 65% to 85%, the minimum increment in ORC efficiency is 2.43% with R227ea, while the maximum is 2.83% with benzene. Though the expander efficiency differs, the ORC efficiency variations with T_{EHST} are similar.

Effect of T_{EHST} of the working fluids on the ORC efficiency at pump efficiency of 50% and 80% is shown in Fig.6. The expander efficiency is 75%.The ORC efficiency is still an increasing function of T_{EHST} at different pump efficiencies, and it decreases with the decrement in pump efficiency. However, the efficiency curves are not parallel, and the influence of pump efficiency on the cycle efficiency varies with the working fluid. When the pump efficiency drops from 80% to 50%, the maximum decrement in ORC efficiency is 0.91% with R227ea, while the minimum is 0.025% with benzene. Fluid of lower critical temperature usually collocates with greater cycle pressure range. For example, the saturation pressure of benzene, R113, R245ca, R245fa, R236ea and RC318 at 100 ºC is 0.18, 0.43, 0.92, 1.26, 1.57 and 2.05 MPa, respectively. Attributed to greater operation pressure, the fluid’s pumping power plays a more noticeable role in the cycle efficiency

[42]. As a result, fluid of lower critical temperature is likely to suffer more from the degradation in pump performance.

Effect of T_{EHST} of the working fluids on the ORC efficiency at condensation temperature of 20°C and 40°C is shown in Fig.7. The evaporation temperature, expander and pump efficiency are the same as the fixed ones in Figs.5 and 6. T_{EHST} of each fluid changes with the condensation temperature. Even so, the ORC efficiency increases with increasing T_{EHST}.

Above all, in the wide range of the expander and pump efficiencies, evaporation and condensation temperature, the ORC efficiency is generally linearly proportional to T_{EHST}. The ORC efficiency is a very strong function of T_{EHST}. The qualitative relationship underscores the potential of T_{EHST} as an indicator of ORC efficiency.

4.2. Comparison among the equivalent hot side temperature and boiling point temperature, critical temperature, Jacobs number and Figure of Merit

In order to clarify the advantages of T_{EHST}, comparison among T_{EHST} and other indicators is made. The indicators include boiling point temperature (T_{bp}), critical temperature (T_c), Jacobs number (Ja) and FOM. The results are shown in Figs.8-11. In each of the figures, the ORC efficiency of a given fluid is constant. The evaporation temperature and condensation temperature are 100 °C and 30 °C. The expander and pump efficiencies are 75% and 65%. The symbols in red color denote T_{EHST}, while those in green color denote the existing indicators. The variation of ORC efficiency with T_{EHST} is much more regular than those with T_{bp}, T_c and Ja. The efficiency is in good relationship with FOM at 100 °C. However, the variation becomes less regular when the evaporation temperature increases to 150 °C as shown in Fig.12. The results show on the same boundary conditions, the ORC

efficiency is directly proportional to T_{EHST} of the working fluids. The relationship between ORC efficiency and T_{EHST} is solid.

The reason why T_{EHST} is able to indicate the ORC efficiency monotonely may be that the cycle is subcritical. In this case, dry fluids are preferable to avoid superheat. The latent heat of condensation is usually dominant in the cooling process. The equivalent cold side temperature (T_{ECST}) is very close to the condensation temperature in spite of the irreversibility in the expander. T_{ECST} is roughly constant as the working fluid changes and T_{EHST} turns out to be the main variable.

4.3. Quantitative relationship between ORC efficiency and the equivalent hot side temperature

The above section has presented the qualitative relationship between ORC efficiency and T_{EHST}. The quantitative relationship is investigated in this section, and error in the efficiency is explicated.

The molecular weight, critical temperature, critical pressure and coefficients in Antoine Equation of the working fluids are listed in Table 4. For R245ca, R227ea and R1234ze, Wagner Equation is used. The coefficients are A_1=-7.340, A_2=0.376, A_3=-0.148, A_4=-12.361 (R245ca), A_1=-7.715, A_2=1.682, A_3=-2.674, A_4=-4.626 (R227ea) and A_1= -7.5046, A_2= 1.5524, A_3= -2.2353, A_4= -4.1018 (R1234ze). For R124, A_1= -7.76544, A_2= 2.36923, A_3= -9.33775, A_4= 217.292 with $\ln p/p_c = T_c/T \cdot (A_1\tau + A_2\tau^{1.5} + A_3\tau^3 + A_4\tau^6)$. For R236ea, modified Riedel Equation is employed and the coefficients are A′=15.9302, B′=-1725.4045, C′=-0.4984, D′=3.2139×10^{-6}, and E′=-2.0096×10^5.

The estimated *a*-value and ORC efficiency are presented in Tables 5 and 6. The condensation temperature of 30 °C, expander efficiency of 75%, pump efficiency of 65%

and generator efficiency of 85% are assumed. In general, fluid of a higher critical temperature offers a lower *a*-value. This may be attributed to a higher ratio of the specific saturation vapor and liquid volumes (v_V / v_L). For example, at 100 °C, v_V / v_L is about 165.7, 88.2, 26.5, 15.5, 7.5 and 1.2 for benzene, acetone, R123, R245fa, isobutane and R227ea, respectively. Given the fluid, *a*-value increases with the increment in the evaporation temperature, which is very significant as the critical temperature is approached. The maximum *a*-value is 9.07% with R227ea at the evaporation temperature of 100 °C. Benzene has the highest ORC efficiency at given evaporation temperature. The relative deviation $\mu(\eta_t)$ of the estimated efficiency from that modelled in the conventional way with REFPROP database is also exhibited in Table 6. Because only one digit after decimal point is reserved, $\mu(\eta_t)$ is expressed as zero for some fluids. Both negative and positive values of $\mu(\eta_t)$ exist. As mentioned in Section 3.4, *a*-value by the model developed in this work and the approximation of q_i will result in an underestimated ORC efficiency, while the approximation of T_{ECST} will lead to an overestimated one. Negative $\mu(\eta_t)$ is usually due to dominant effect by *a*-value and $q_i = q_{i,id}$, which seems valid for slightly dry and isentropic fluids such as transbutene, isobutene, isobutane and cisbutene. Positive $\mu(\eta_t)$ is accompanied with dry fluids such as cyclohexane, R113 and isopentane, for which T_{ECST} is higher than the condensation temperature (T_1) owing to the superheated exhaust from the expander.

In most cases, $\mu(\eta_t)$ is within ±2%. R245fa is a hydro-fluorocarbon (HFC) with zero Ozone Depletion Potential (ODP). Nowadays, it is a common working fluid in commercial ORC installations such as GE CleanCycle™ [43] and Verdicorp ORC model [44]. The estimated ORC efficiency using this fluid shows high accuracy, and the relative bias is

from -0.3% to 0.5%. Among the fluids, the deviation of the estimated efficiency is largest in the presence of isopentane. It is a highly dry working fluid. For example, given the expander efficiency of 0.75 and evaporation and condensation temperature of 150 °C and 30 °C, the fluid leaving the expander will be at 87 °C with a degree of superheat of 57 °C. The high degree of superheat causes relatively appreciable error in approximating T_{ECST}.

Aside from the basic thermodynamic processes represented in Fig.1, another type of ORC with a degree of superheat (ΔT_{super}) at the expander inlet is taken into consideration for a comprehensive evaluation of the new model. In the superheat cycle, state points 1, 2, 2s and 4′ do not change, while state point 3 moves upward by 5 °C along the isobaric curve. State points 4 and 4s change consequently. Table 7 lists T_{EHST} of the working fluids in the evaporation temperature range from 100 °C to 150 °C. The estimated ORC efficiency and relative error are provided in Table 8 under the similar assumption made in Table 6. Resulting from 5 °C of ΔT_{super}, T_{EHST} goes up when the evaporation temperature and working fluid are allocated in comparison with that in Table 6. The increment becomes more noticeable at higher evaporation temperature and for fluids of lower critical temperature. Unlike T_{EHST} and $\eta_{t,EHST}$, the estimated *a*-value is not affected by ΔT_{super} because of unvaried integration path and pressure at a given evaporation temperature.

$\mu(\eta_t)$ in Table 8 is within an interval of (-1.4%, +4.6%). The developed ORC efficiency model seems to have a lower accuracy in the superheat ORC. There can be two reasons. The first one is that for many dry fluids, a degree of superheat at the expander inlet does not elevate the ORC efficiency [45]. In fact, the ORC efficiency of isopentane decreases from 12.43% to 12.41% as ΔT_{super} climbs from 0 °C to 5 °C. On the contrary, T_{EHST} is increased by ΔT_{super} and this leads to a higher efficiency based on the proposed model. The

positive deviation of $\eta_{t,EHST}$ from $\eta_{t,REFP}$ hence becomes larger. The second reason lies in the diverse error in *a*-value as ΔT_{super} changes. Take butene for example. At an evaporation temperature of 140 °C, the fluid after ideal expansion is at binary phase state with a quality of about 0.98 for a basic ORC. In this situation, T_{ECST} is equal to the condensation temperature. And the error caused by the approximation of q_i and *a*-value is primary. The error in $q_i \approx q_{id}$ is in weak relation with ΔT_{super} regarding the constant pump efficiency, while the error in *a*-value varies significantly. With the increment in ΔT_{super} the difference of $v\big|_p - v_s\big|_p$ increases, and it is likely to co-occur with a lower estimated ORC efficiency as mentioned in Section 3.4.3. Therefore, the negative deviation of $\eta_{t,EHST}$ for butene changes from -0.7% without superheat to -1.4% at ΔT_{super} of 5 °C.

It needs to be emphasized that isentropic and dry fluids are favorable in the ORC, and superheat at the expander inlet should be avoided [8, 46]. In the presence of superheat cycle, thermodynamic parameters of the working fluid at superheat state are also required, which will make the proposed model less convenient.

5. Case study

A newly developed refrigerant, Hydro-Fluoro-Olefin HFO1336mzzZ (cis-$CF_3CH=CHCF_3$) is exemplified. It is a dry fluid, and has no ODP and extremely good thermal stability at temperature up to 250°C [47]. Its GWP is only 9, which is much lower than that of the widely used R245fa (about 1030). Some properties are listed in Table 9. HFO1336mzzZ exhibits attractive physical characteristics for use in low and medium temperature ORC applications.

The exploration of thermodynamic performance of this new working fluid in the potential ORC application regarding the conventional efficiency model will require a detailed knowledge of its PVT behavior, but experimental data for this compound in literature are rare. So far studies on the performance of HFO1336mzzZ as an ORC working fluid have been based on data from DuPont, which may be incomplete and are not available in open literature [48]. Comprehensive information about this fluid is unavailable on the database of REFPROP and CoolProp. Though it is difficult to obtain the accurate thermodynamic parameters in the wide temperature and pressure ranges at gas state, the parameters at saturation liquid/vapor state are easier to determine. The experiment work on saturation parameters is less cumbersome. The saturation temperature-pressure and temperature-entropy (*T*-*s*) graphs of HFO1336mzzZ are accessible [49, 50]. Besides, the vapor-liquid equilibria of this fluid can be predicted by molecular simulations. For example, a transferable force field model has been applied for simulation studies on saturated vapor pressure, vapor density and liquid density and heats of vaporization of fluoropropenes, and the simulated data generally agree well with available experimental data [51].

The specific liquid enthalpy ($h_{l,s}$), vapor enthalpy ($h_{v,s}$), liquid entropy ($s_{l,s}$), vapor entropy ($s_{v,s}$), vapor volume ($v_{v,s}$) and pressure (p_s) of HFO1336mzzZ at the saturation state are listed in Table 10. The saturation liquid density at 30 °C is 1352 kg/m^3, which is useful for the ascertainment of pump power. With the thermodynamic parameters at liquid-vapor equilibrium state, the ORC efficiency can be calculated by the new model built in this work. Some results are listed in Table 11. R245fa is referenced. The efficiencies of the expander and generator are 75% and 85%. The condensation temperature is 30 °C. Basic ORC without superheat at the expander inlet is under discussion. Compared with

R245fa, HFO1336mmZ has a lower *a*-value. For an inefficient pumping process, the exergy loss in case of HFO1336mmZ will be less appreciable than that with R245fa. On the other hand, T_{EHST} of HFO1336mmZ is lower in a wide range of ORC evaporation temperature, with the exception of 150 ^{o}C which is close to the critical temperature of R245fa. Due to the competitive effects of *a*-value and T_{EHST}, the ORC efficiencies of HFO1336mmZ and R245fa are comparable. Given a modest pump efficiency of 65%, HFO1336mmZ has no efficiency superiority over R245fa unless the evaporation temperature exceeds 130 ^{o}C. The superiority is more appreciable with less efficient pump and higher operating temperature.

6. Conclusions

T_{EHST} is determined by the thermodynamic parameters at the liquid-vapor equilibrium state. Given the condensation temperature and working fluid, it is a function with respect to the evaporation temperature. This indicator is strongly related with the ORC efficiency. On the same operating conditions, fluid of higher T_{EHST} generally leads to more efficient heat-to-power conversion. This rule is applicable in a wide range of hot and cold side temperatures, expander and pump efficiencies. It is concluded that T_{EHST} provides a more universal guideline on the ORC efficiency assessment as compared to some existing indicators such as boiling point temperature, critical temperature, Jacobs number and Figure of Merit.

T_{EHST} generally increases with the increment in the evaporation temperature for each fluid. Nevertheless, as the evaporation temperature approaches to critical temperature of the fluid, T_{EHST} increases slowly and may even decrease. This explains why the cycle efficiencies of some fluids decrease when the evaporation temperature gets close to their critical temperatures.

A new ORC efficiency model is built with the assistance of T_{EHST}. In contrast to the conventional model, the efficiency in the new model is determined by the liquid-vapor equilibrium data of the fluid and it is unnecessary to get information on parameters at superheat state. An error compensation method is developed by the approximation of *a*-value and T_{ECST}. On the use of twenty-seven fluids, the ORC efficiency obtained by the hypothetical model is in good agreement with the actual. The relative error is from -0.7% to 3.4%. The largest deviation occurs when the highly dry fluid (isopentane) is employed. For more than half of the investigated fluids, the relative error is within $\pm 0.6\%$.

The accuracy of the proposed model becomes relatively lower in the situation of 5 ^{o}C of superheat at the expander inlet. The deviation of estimated efficiency from the real is enlarged due to the unwanted overheat and has a value up to 4.6%.

A case study using the newly developed fluid of HFO-1336mzz-Z is conducted with expander and generator efficiency of 75% and 85%. Though this fluid is promising in terms of the environmental issues, it has efficiency superiority over R245fa only at relatively high evaporation temperature (>130 ^{o}C) or relatively lower pump efficiency (<65%).

Acknowledgment

This study was sponsored by the National Science Foundation of China (51476159, 51378483, 51206154), Project of EU Marie Curie International Incoming Fellowships (703746), Anhui Provincial Natural Science Foundation (1608085QE96), CAS-TWAS presidential fellowship program, and Dongguan Innovative Research Team Program (2014607101008).

References

1. Tchanche, B.F., et al., *Low-grade heat conversion into power using organic Rankine cycles – A review of various applications.* Renewable and Sustainable Energy Reviews, 2011. **15**(8): p. 3963-3979.
2. Wang, J., et al., *Thermodynamic analysis and optimization of an (organic Rankine cycle) ORC using low grade heat source.* Energy, 2013. **49**(0): p. 356-365.
3. Chen, H., D.Y. Goswami, and E.K. Stefanakos, *A review of thermodynamic cycles and working fluids for the conversion of low-grade heat.* Renewable and Sustainable Energy Reviews, 2010. **14**(9): p. 3059-3067.
4. Quoilin, S., *Sustainable Energy Conversion Through the Use of Organic Rankine Cycles for Waste Heat Recovery and Solar Applications*. 2011, University of Liège (Belgium.
5. Maizza, V. and A. Maizza, *Working fluids in non-steady flows for waste energy recovery systems.* Applied Thermal Engineering, 1996. **16**(7): p. 579-590.
6. Papadopoulos, A.I., M. Stijepovic, and P. Linke, *On the systematic design and selection of optimal working fluids for Organic Rankine Cycles.* Applied Thermal Engineering, 2010. **30**(6): p. 760-769.
7. Wang, J., J. Zhang, and Z. Chen, *Molecular entropy, thermal efficiency, and designing of working fluids for organic Rankine cycles.* International Journal of Thermophysics, 2012. **33**(6): p. 970-985.
8. Saleh, B., et al., *Working fluids for low-temperature organic Rankine cycles.* Energy, 2007. **32**(7): p. 1210-1221.
9. Maizza, V. and A. Maizza, *Unconventional working fluids in organic Rankine-cycles for waste energy recovery systems.* Applied thermal engineering, 2001. **21**(3): p. 381-390.
10. Mikielewicz, D. and J. Mikielewicz, *A thermodynamic criterion for selection of working fluid for subcritical and supercritical domestic micro CHP.* Applied Thermal Engineering, 2010. **30**(16): p. 2357-2362.
11. Kuo, C.-R., et al., *Analysis of a 50kW organic Rankine cycle system.* Energy, 2011. **36**(10): p. 5877-5885.
12. Lai, N.A., M. Wendland, and J. Fischer, *Working fluids for high-temperature organic Rankine cycles.* Energy, 2011. **36**(1): p. 199-211.

13. Aljundi, I.H., *Effect of dry hydrocarbons and critical point temperature on the efficiencies of organic Rankine cycle.* Renewable Energy, 2011. **36**(4): p. 1196-1202.
14. Heberle, F. and D. Brüggemann, *Exergy based fluid selection for a geothermal Organic Rankine Cycle for combined heat and power generation.* Applied Thermal Engineering, 2010. **30**(11): p. 1326-1332.
15. Liu, B.-T., K.-H. Chien, and C.-C. Wang, *Effect of working fluids on organic Rankine cycle for waste heat recovery.* Energy, 2004. **29**(8): p. 1207-1217.
16. He, C., et al., *The optimal evaporation temperature and working fluids for subcritical organic Rankine cycle.* Energy, 2012. **38**(1): p. 136-143.
17. Desideri, A., et al., *Experimental comparison of organic fluids for low temperature ORC (organic Rankine cycle) systems for waste heat recovery applications.* Energy, 2016. **97**: p. 460-469.
18. He, C., et al., *A new selection principle of working fluids for subcritical organic Rankine cycle coupling with different heat sources.* Energy, 2014. **68**: p. 283-291.
19. Lecompte, S., et al., *Part load based thermo-economic optimization of the Organic Rankine Cycle (ORC) applied to a combined heat and power (CHP) system.* Applied Energy, 2013. **111**: p. 871-881.
20. Cataldo, F., et al., *Fluid selection of Organic Rankine Cycle for low-temperature waste heat recovery based on thermal optimization.* Energy, 2014. **72**: p. 159-167.
21. Song, J., et al., *Thermodynamic analysis and performance optimization of an ORC (Organic Rankine Cycle) system for multi-strand waste heat sources in petroleum refining industry.* Energy, 2014. **71**: p. 673-680.
22. Zhai, H., L. Shi, and Q. An, *Influence of working fluid properties on system performance and screen evaluation indicators for geothermal ORC (organic Rankine cycle) system.* Energy, 2014. **74**: p. 2-11.
23. Xue, X., et al., *Thermodynamic analysis and optimization of a two-stage organic Rankine cycle for liquefied natural gas cryogenic exergy recovery.* Energy, 2015. **83**: p. 778-787.
24. Hajabdollahi, Z., et al., *Thermo-economic environmental optimization of Organic Rankine Cycle for diesel waste heat recovery.* Energy, 2013. **63**: p. 142-151.

25. Astolfi, M., et al., *Binary ORC (organic Rankine cycles) power plants for the exploitation of medium–low temperature geothermal sources–Part A: Thermodynamic optimization.* Energy, 2014. **66**: p. 423-434.
26. Astolfi, M., et al., *Binary ORC (Organic Rankine Cycles) power plants for the exploitation of medium–low temperature geothermal sources–Part B: Techno-economic optimization.* Energy, 2014. **66**: p. 435-446.
27. Yang, M.-H. and R.-H. Yeh, *Economic performances optimization of an organic Rankine cycle system with lower global warming potential working fluids in geothermal application.* Renewable Energy, 2016. **85**: p. 1201-1213.
28. Borsukiewicz-Gozdur, A., *Exergy analysis for maximizing power of organic Rankine cycle power plant driven by open type energy source.* Energy, 2013. **62**: p. 73-81.
29. Wang, E., et al., *Study of working fluid selection of organic Rankine cycle (ORC) for engine waste heat recovery.* Energy, 2011. **36**(5): p. 3406-3418.
30. Heberle, F., M. Preißinger, and D. Brüggemann, *Zeotropic mixtures as working fluids in Organic Rankine Cycles for low-enthalpy geothermal resources.* Renewable Energy, 2012. **37**(1): p. 364-370.
31. Feng, Y., et al., *Thermoeconomic comparison between pure and mixture working fluids of organic Rankine cycles (ORCs) for low temperature waste heat recovery.* Energy Conversion and Management, 2015. **106**: p. 859-872.
32. Maraver, D., et al., *Systematic optimization of subcritical and transcritical organic Rankine cycles (ORCs) constrained by technical parameters in multiple applications.* Applied energy, 2014. **117**: p. 11-29.
33. Toffolo, A., et al., *A multi-criteria approach for the optimal selection of working fluid and design parameters in Organic Rankine Cycle systems.* Applied Energy, 2014. **121**: p. 219-232.
34. Shu, G., et al., *Alkanes as working fluids for high-temperature exhaust heat recovery of diesel engine using organic Rankine cycle.* Applied Energy, 2014. **119**: p. 204-217.

35. Wang, J., et al., *Multi-objective optimization of an organic Rankine cycle (ORC) for low grade waste heat recovery using evolutionary algorithm.* Energy Conversion and Management, 2013. **71**: p. 146-158.
36. Mago, P.J., et al., *An examination of regenerative organic Rankine cycles using dry fluids.* Applied Thermal Engineering, 2008. **28**(8): p. 998-1007.
37. Srinivasan, K.K., P.J. Mago, and S.R. Krishnan, *Analysis of exhaust waste heat recovery from a dual fuel low temperature combustion engine using an Organic Rankine Cycle.* Energy, 2010. **35**(6): p. 2387-2399.
38. Chen, Q., J. Xu, and H. Chen, *A new design method for organic Rankine cycles with constraint of inlet and outlet heat carrier fluid temperatures coupling with the heat source.* Applied Energy, 2012. **98**: p. 562-573.
39. Hung, T., T. Shai, and S. Wang, *A review of organic Rankine cycles (ORCs) for the recovery of low-grade waste heat.* Energy, 1997. **22**(7): p. 661-667.
40. Frenkel, D. and B. Smit, *Understanding molecular simulation: from algorithms to applications*. Vol. 1. 2001: Academic press.
41. Martin, M.G., *MCCCS Towhee: a tool for Monte Carlo molecular simulation.* Molecular Simulation, 2013. **39**(14-15): p. 1212-1222.
42. Borsukiewicz-Gozdur, A., *Pumping work in the organic Rankine cycle.* Applied Thermal Engineering, 2013. **51**(1): p. 781-786.
43. *GE - Model Clean Cycle 125™ - Organic Rankine Cycle (ORC) Systems*. 2015.12.11]; Available from: http://www.environmental-expert.com/products/ge-model-clean-cycle-125-organic-rankine-cycle-orc-systems-177085.
44. *Verdicorp's Organic Rankine Cycle System.* . 2015.11.10]; Available from: http://verdicorp.com/orc.html.
45. Hung, T.-C., T. Shai, and S. Wang, *A review of organic Rankine cycles (ORCs) for the recovery of low-grade waste heat.* Energy, 1997. **22**(7): p. 661-667.
46. Hung, T.-C., *Waste heat recovery of organic Rankine cycle using dry fluids.* Energy Conversion and Management, 2001. **42**(5): p. 539-553.
47. Juhasz JR, Simoni LD. A review of potential working fluids for low temperature organic Rankine cycles in waste heat recovery. The third edition of the

International Seminar on ORC Power Systems (ASME ORC 2015),Brussels, 12 to 14 October, 2015.

48. Raabe, G., *Molecular Simulation Studies on the Vapor–Liquid Equilibria of the cis-and trans-HCFO-1233zd and the cis-and trans-HFO-1336mzz.* Journal of Chemical & Engineering Data, 2015. **60**(8): p. 2412-2419.
49. Molés, F., et al., *Low GWP alternatives to HFC-245fa in Organic Rankine Cycles for low temperature heat recovery: HCFO-1233zd-E and HFO-1336mzz-Z.* Applied Thermal Engineering, 2014. **71**(1): p. 204-212.
50. Kontomaris K. HFO-1336mzz-Z: High Temperature Chemical Stability and Use as A Working Fluid in Organic Rankine Cycles. International Refrigeration and Air Conditioning Conference, Purdue University, 2014.
51. Raabe, G., *Molecular modeling of fluoropropene refrigerants.* The Journal of Physical Chemistry B, 2012. **116**(19): p. 5744-5751.
52. Eon, C., C. Pommier, and G. Guiochon, *Vapor pressures and second virial coefficients of some five-membered heterocyclic derivatives.* Journal of Chemical & Engineering Data, 1971. **16**(4): p. 408-410.
53. Kerns, W., R. Anthony, and P. Eubank. *Volumetric properties of cyclohexane vapor*. in *AIChE Symp. Ser*. 1974.
54. Ambrose, D., C. Sprake, and R. Townsend, *Thermodynamic properties of organic oxygen compounds XXXIII. The vapour pressure of acetone.* The Journal of Chemical Thermodynamics, 1974. **6**(7): p. 693-700.
55. Goodwin, A., et al., *The vapor pressure of 1, 1-dichloro-2, 2, 2-trifluoroethane (R123).* International journal of thermophysics, 1992. **13**(6): p. 999-1009.
56. Di Nicola, G. and G. Passerini, *Saturated pressure and gas phase PVT data for 1, 1, 2, 2, 3-pentafluoropropane (R-245ca).* Journal of Chemical & Engineering Data, 2002. **47**(4): p. 882-886.
57. Di Nicola, G., *Vapor pressure and gas phase P-V-T data for 1, 1, 1, 3, 3-pentafluoropropane (R-245fa).* Journal of Chemical & Engineering Data, 2001. **46**(6): p. 1619-1622.

58. Di Nicola, G. and G. Giuliani, *Vapor Pressure and P-V-T Measurements for 1, 1, 1, 2, 3, 3-Hexafluoropropane (R-236ea).* Journal of Chemical & Engineering Data, 2000. **45**(6): p. 1075-1079.
59. Das, T.R., C.O. Reed Jr, and P.T. Eubank, *PVT [pressure-volume-temperature] surface and thermodynamic properties of isobutane.* Journal of Chemical and Engineering Data, 1973. **18**(3): p. 253-262.
60. Di Nicola, G., et al., *Saturated Pressure and P-V-T Measurements for 1, 1, 1, 3, 3, 3-Hexafluoropropane (R-236fa).* Journal of Chemical & Engineering Data, 1999. **44**(4): p. 696-700.
61. Di Nicola, G., *PVT Behavior of 1, 1, 1, 2, 3, 3, 3-Heptafluoropropane (R227ea).* Journal of Chemical & Engineering Data, 2003. **48**(5): p. 1332-1336.

Figure Legend

Fig.1. T-*s* diagram of ORC

Fig.2. Variation of T_{ECST} with the degree of superheat at the expander outlet

Fig.3. Influence of T_{EHST} of the working fluids on the ORC efficiency at evaporation temperature of 100, 120 and 150 ^{o}C

Fig. 4. Variation of T_{EHST} of the working fluids with the evaporation temperature

Fig. 5. Influence of T_{EHST} of the working fluids on the ORC efficiency at expander efficiency of 65% and 85%

Fig. 6. Influence of T_{EHST} of the working fluids on the ORC efficiency at pump efficiency of 50% and 80%

Fig. 7. Influence of T_{EHST} of the working fluids on the ORC efficiency at condensation temperature of 20^{o}C and 40^{o}C

Fig. 8. Effect of T_{ESHT} and boiling point temperature on the ORC efficiency of working fluids

Fig. 9. Effect of T_{ESHT} and critical temperature on the ORC efficiency of working fluids

Fig. 10. Effect of T_{ESHT} and Jacobs number on the ORC efficiency of working fluids

Fig.11. Effect of T_{ESHT} and Figure of Merit on the ORC efficiency of working fluids at evaporation and condensation temperature of 100^{o}C and 30^{o}C respectively

Fig. 12. Effect of T_{ESHT} and Figure of Merit on the ORC efficiency of working fluids at evaporation and condensation temperature of 150^{o}C and 30^{o}C respectively

Table Legend

Table 1. T_{EHST} of the working fluids in the evaporation temperature range from100 ^{o}C to 150^{o}C, unit: ^{o}C

Table 2. Error caused by approximating the equivalent cold side temperature, unit: ^{o}C

Table 3. Relative error in approximating the heat input, unit: %

Table 4. Some properties of the working fluids

Table 5. Estimated *a*-value of the working fluids in the evaporation temperature range from 100 ^{o}C to 150^{o}C, unit: %

Table 6. Estimated efficiency of the working fluids unit: %

Table 7. TEHST of the working fluids with a degree of superheat of 5 ^{o}C at the expander inlet, unit: ^{o}C

Table 8. Estimated efficiency of the working fluids with a degree of superheat of 5 ^{o}C at the expander inlet, unit: %

Table 9. Some properties of HFO1336mzzZ

Table 10. Thermodynamic parameters of HFO1336mzzZ at saturation state

Table 11. Estimated efficiency of HFO1336mmZ compared with R245fa

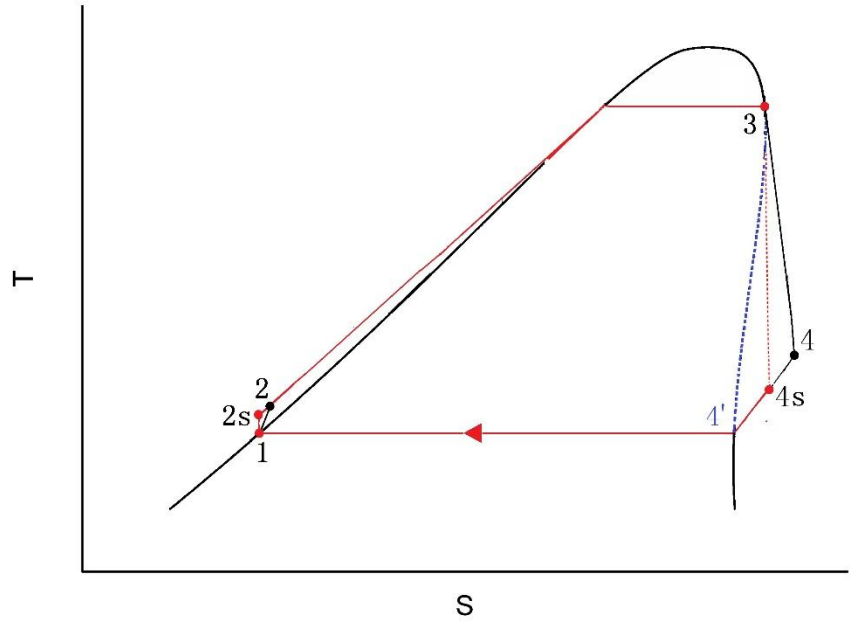

Fig.1. *T-s* diagram of ORC

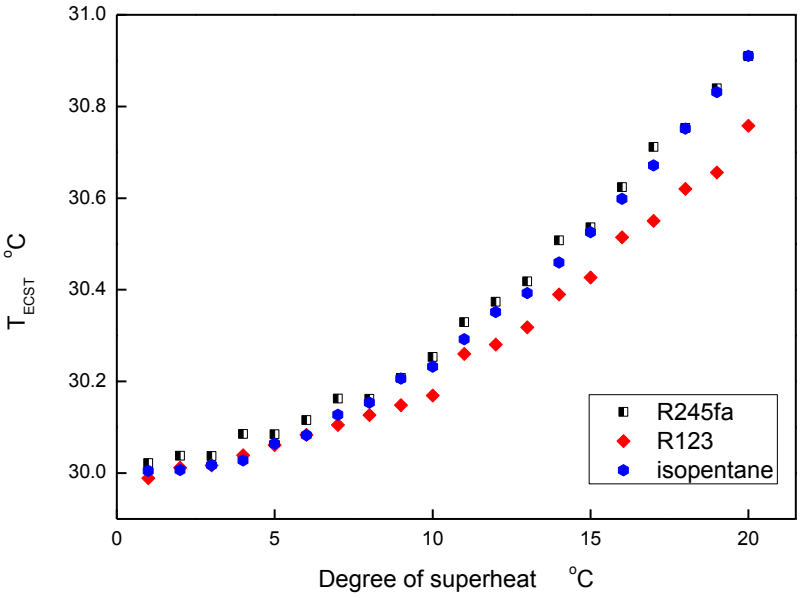

Fig.2. Variation of T_{ECST} with the degree of superheat at the expander outlet

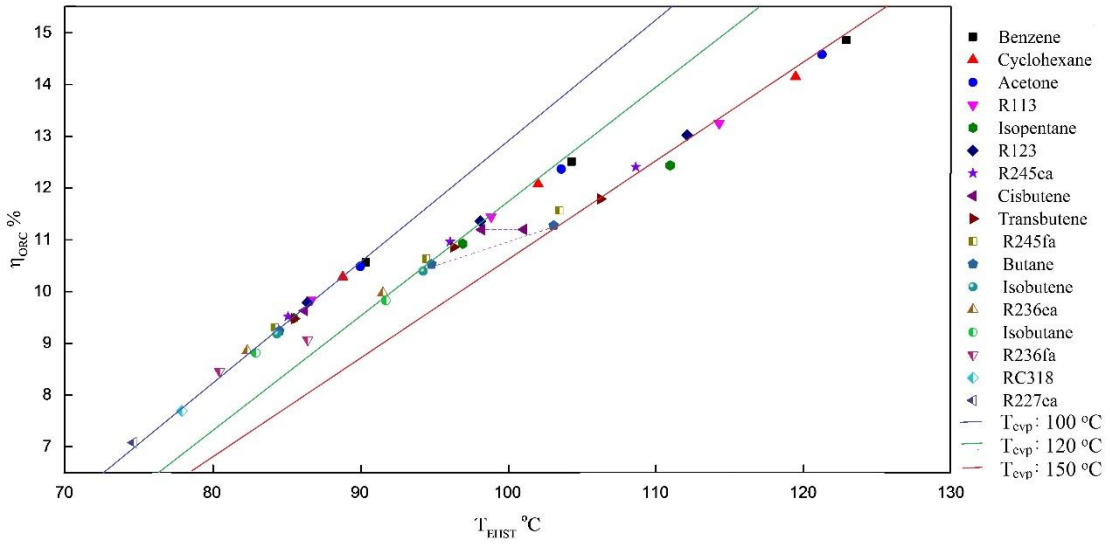

Fig.3. Influence of T_{EHST} of the working fluids on the ORC efficiency at evaporation temperature of 100, 120 and 150 °C

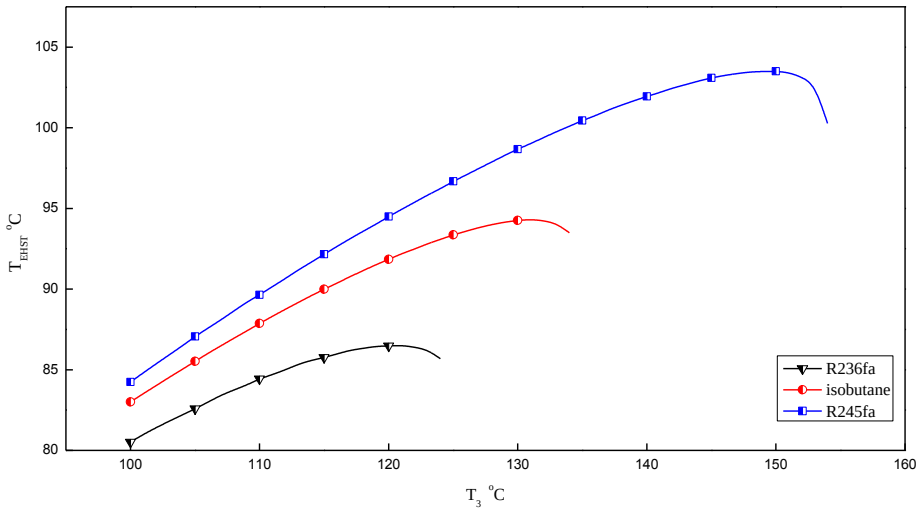

Fig. 4. Variation of T_{EHST} of the working fluids with the evaporation temperature

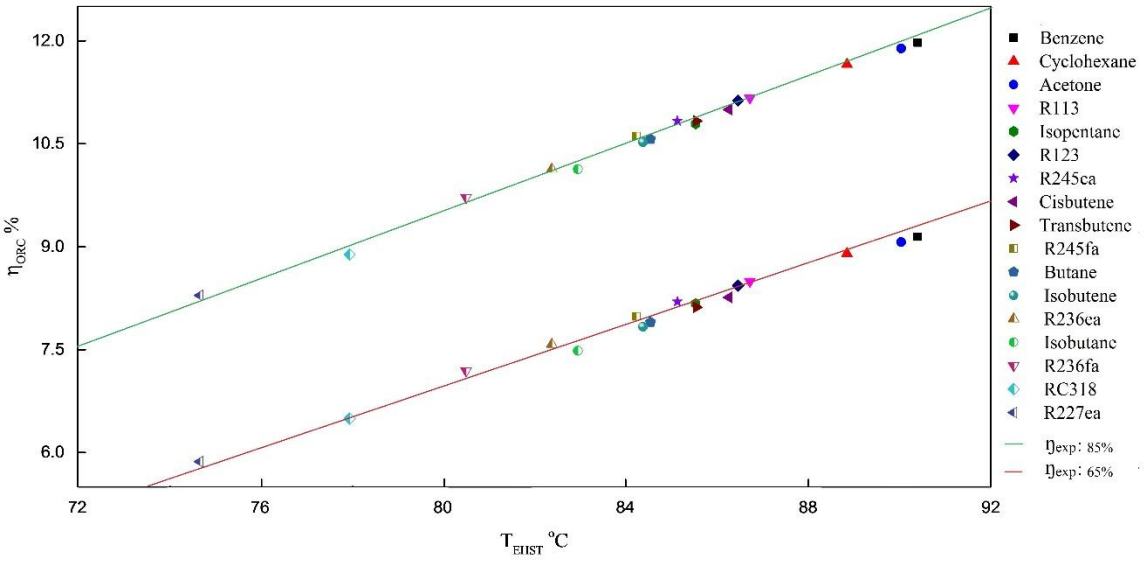

Fig. 5. Influence of T_{EHST} of the working fluids on the ORC efficiency at expander efficiency of 65% and 85%

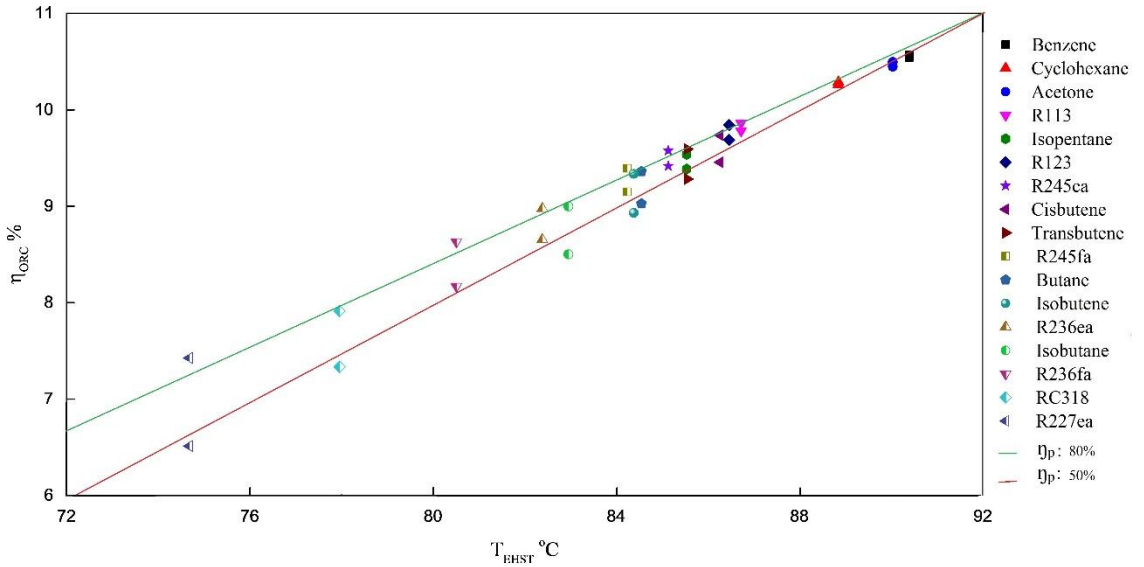

Fig. 6. Influence of T_{EHST} of the working fluids on the ORC efficiency at pump efficiency of 50% and 80%

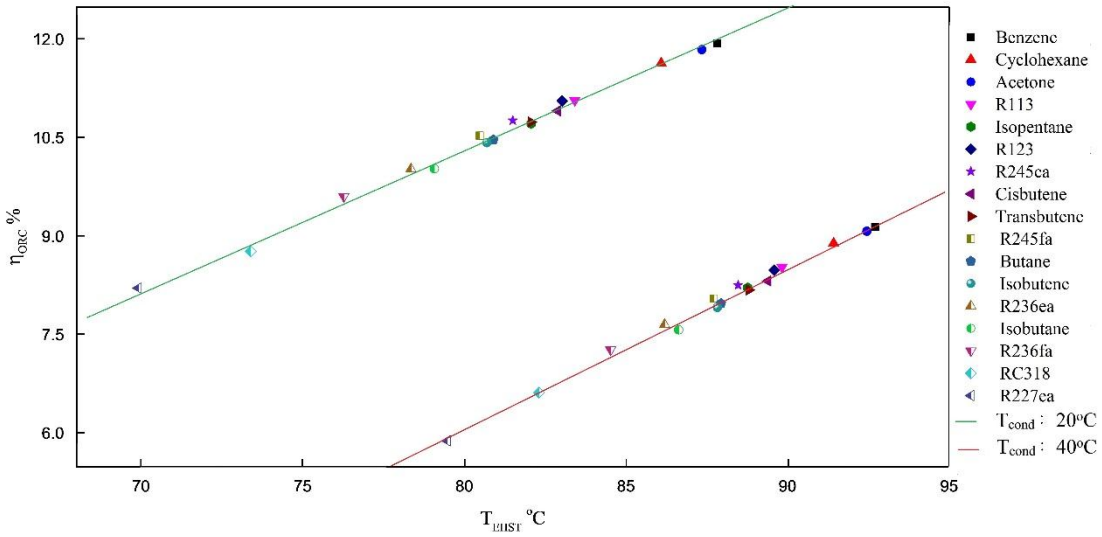

Fig. 7. Influence of T_{EHST} of the working fluids on the ORC efficiency at condensation temperature of 20°C and 40°C

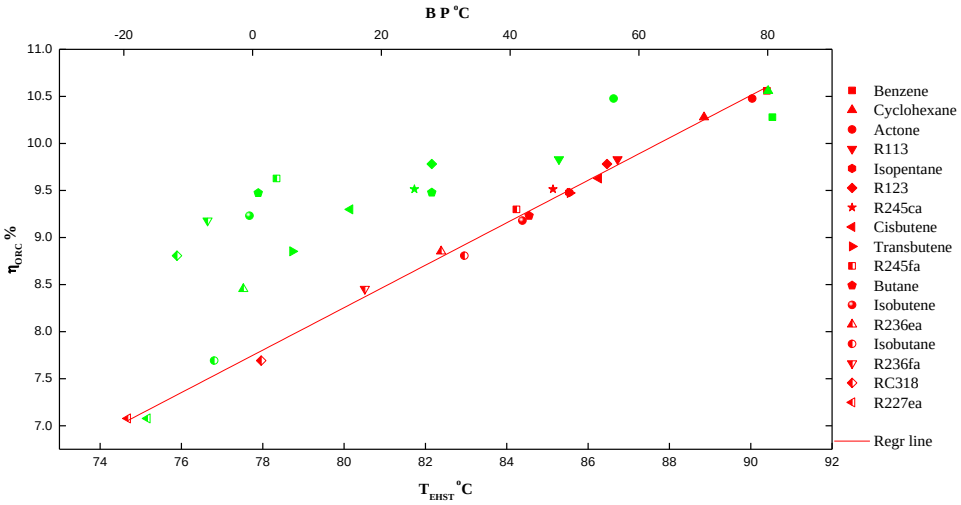

Fig. 8. Effects of T_{ESHT} and boiling point temperature on the ORC efficiency of working fluids

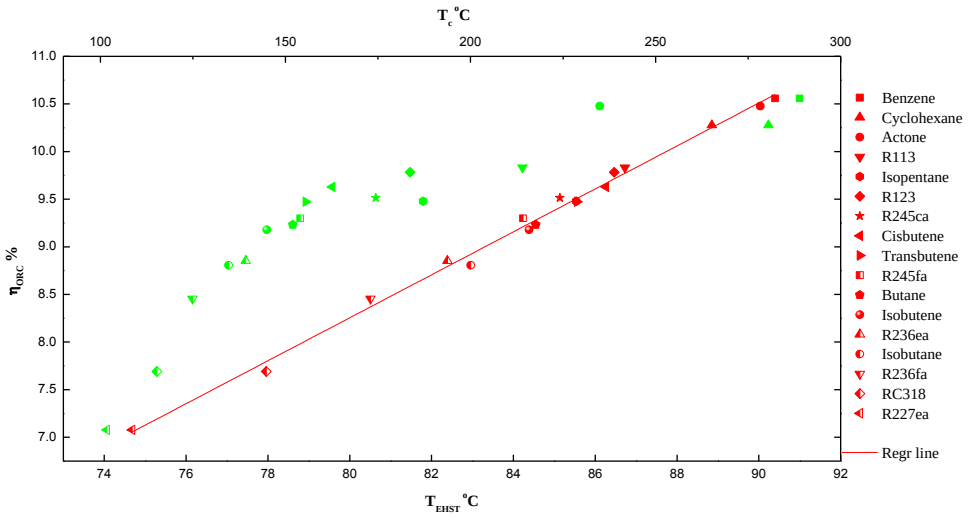

Fig. 9. Effects of T_{ESHT} and critical temperature on the ORC efficiency of working fluids

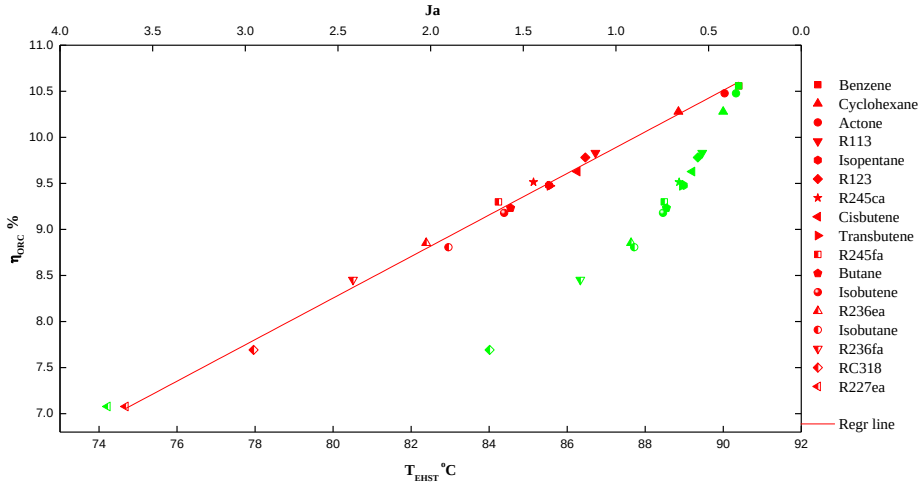

Fig. 10. Effects of T_{ESHT} and Jacobs number on the ORC efficiency of working fluids

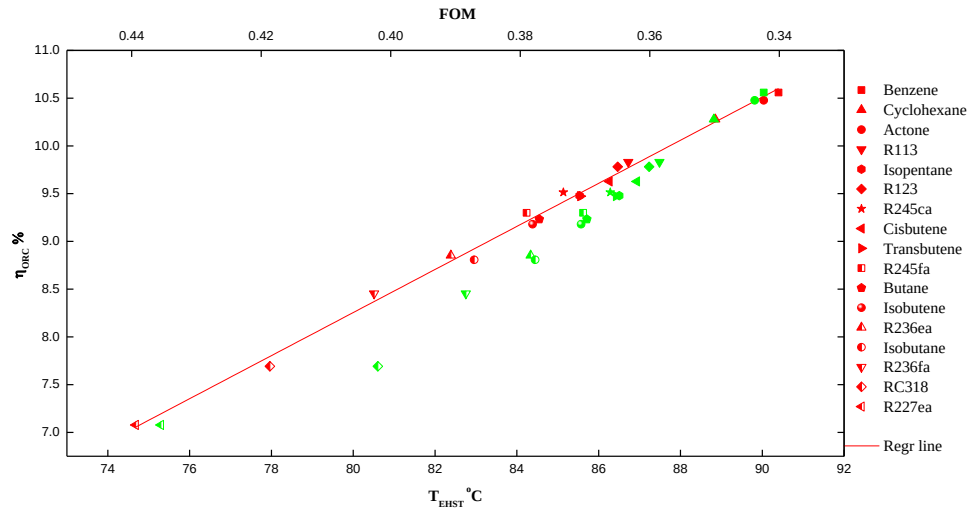

Fig.11. Effects of T_{ESHT} and Figure of Merit on the ORC efficiency of working fluids at evaporation and condensation temperature of 100°C and 30°C respectively

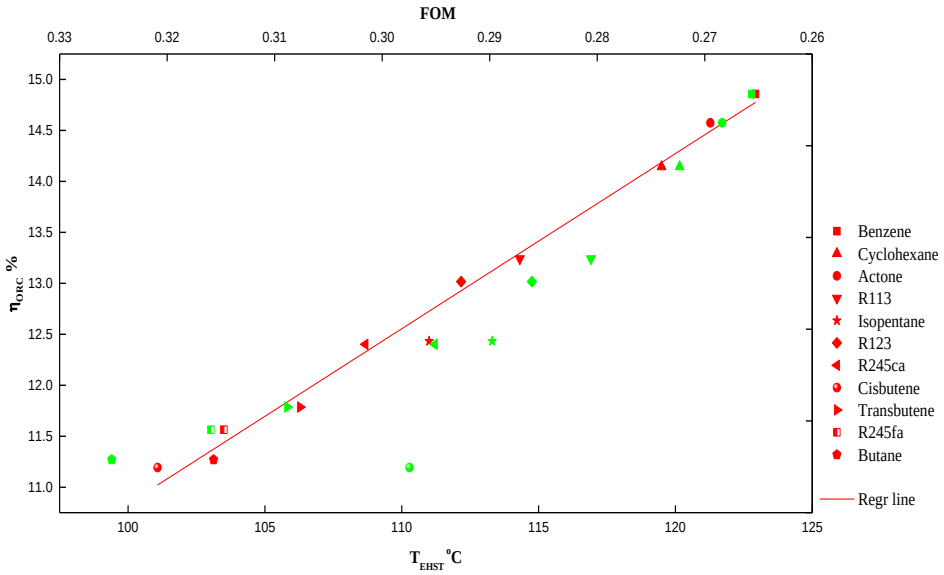

Fig. 12. Effects of T_{ESHT} and Figure of Merit on the ORC efficiency of working fluids at evaporation and condensation temperature of 150°C and 30°C respectively

Table 1. T_{EHST} of the working fluids in the evaporation temperature range from 100 °C to 150°C, unit: °C

Fluid	Evaporation temperature, °C										
	100	105	110	115	120	125	130	135	140	145	150
Toluene	90.1	93.7	97.2	100.6	104.0	107.3	110.5	113.6	116.7	119.7	122.6
Benzene	90.4	94.0	97.5	101.0	104.3	107.6	110.8	114.0	117.0	120.0	122.9
Cyclohexane	88.9	92.3	95.6	98.9	102.1	105.2	108.2	111.1	114.0	116.8	119.5
Cyclopentane	89.1	92.6	95.9	99.2	102.3	105.4	108.4	111.3	114.1	116.9	119.5
Acetone	90.0	93.6	97.0	100.4	103.6	106.8	109.9	112.9	115.8	118.6	121.3
R113	86.7	89.9	93.0	96.0	98.9	101.7	104.4	107.0	109.5	112.0	114.3
R141b	88.0	91.3	94.5	97.6	100.6	103.5	106.3	109.0	111.6	114.0	116.4
R11	88.3	91.7	94.9	98.0	101.0	103.9	106.7	109.3	111.9	114.3	116.7
Pentane	86.0	89.1	92.1	94.9	97.7	100.4	103.0	105.5	107.9	110.2	112.4
Isopentane	85.5	88.5	91.5	94.3	97.0	99.6	102.1	104.5	106.8	108.9	111.0
R123	86.5	89.6	92.5	95.4	98.2	100.8	103.3	105.7	108.0	110.1	112.2
R245ca	85.1	88.1	90.9	93.6	96.1	98.6	100.9	103.1	105.1	107.0	108.7
Cisbutene	86.3	89.3	92.1	94.9	97.5	99.9	102.2	104.3	106.2	107.9	109.3
Transbutene	85.6	88.5	91.2	93.9	96.3	98.7	100.8	102.7	104.3	105.6	106.3
R245fa	84.2	87.1	89.6	92.2	94.5	96.7	98.7	100.4	101.9	103.1	103.5
Butane	84.5	87.3	90.0	92.5	94.9	97.0	99.0	100.8	102.3	103.3	103.1
Butene	84.7	87.5	90.1	92.6	94.9	96.9	98.7	100.1	101.1	100.3	
R114	83.1	85.7	88.2	90.5	92.7	94.6	96.3	97.6	98.6	98.5	

Isobutene	84.4	87.1	89.7	92.1	94.3	96.3	98.0	99.3	100.1
R236ea	82.4	84.9	87.3	89.5	91.6	93.4	95.0	96.2	
R142b	84.2	86.9	89.3	91.6	93.5	95.2	96.3	96.3	
Isobutane	83.0	85.5	87.8	89.9	91.8	93.3	94.2		
R236fa	80.5	82.6	84.4	85.8	86.5				
R124	81.5	83.7	85.6	86.9	87.2				
RC318	78.0	79.7	80.9						
R1234ze	79.1	80.3							
R227ea	74.7								

Table 2. Error caused by approximating the equivalent cold side temperature, unit: ºC

Fluid	Evaporation temperature, ºC										
	100	105	110	115	120	125	130	135	140	145	150
Toluene	0.01	0.03	0.05	0.08	0.11	0.15	0.20	0.27	0.34	0.41	0.50
Benzene	0.00	0.00	0.00	0.00	0.00	0.00	0.00	0.00	0.01	0.02	0.04
Cyclohexane	0.29	0.37	0.47	0.57	0.69	0.84	0.99	1.16	1.34	1.54	1.75
Cyclopentane	0.03	0.04	0.07	0.09	0.13	0.17	0.22	0.28	0.33	0.40	0.48
Acetone	0.00	0.00	0.00	0.00	0.00	0.00	0.00	0.00	0.00	0.00	0.00
R113	0.68	0.81	0.93	1.07	1.21	1.36	1.52	1.67	1.84	1.99	2.16
R141b	0.05	0.05	0.06	0.08	0.08	0.10	0.12	0.14	0.15	0.17	0.19
R11	0.00	0.00	0.00	0.00	0.00	0.00	0.00	0.00	0.00	0.00	0.00
pentane	0.98	1.15	1.32	1.51	1.71	1.92	2.14	2.36	2.58	2.81	3.03
Isopentane	1.14	1.32	1.51	1.72	1.94	2.17	2.40	2.63	2.85	3.08	3.29
R123	0.20	0.23	0.27	0.31	0.35	0.39	0.41	0.46	0.47	0.50	0.49
R245ca	0.54	0.62	0.70	0.79	0.89	0.97	1.03	1.10	1.16	1.18	1.18
Cisbutene	0.00	0.01	0.01	0.01	0.01	0.01	0.00	0.00	0.00	0.00	0.00
Transbutene	0.07	0.08	0.09	0.09	0.08	0.08	0.06	0.05	0.02	0.00	0.00
R245fa	0.37	0.42	0.45	0.49	0.53	0.54	0.54	0.52	0.44	0.34	0.16
Butane	0.39	0.43	0.48	0.52	0.54	0.55	0.54	0.50	0.42	0.28	0.05
Butene	0.05	0.05	0.05	0.04	0.03	0.02	0.01	0.00	0.00		
R114	0.77	0.84	0.91	0.95	0.96	0.97	0.91	0.81	0.59		
Isobutene	0.09	0.10	0.11	0.10	0.08	0.06	0.03	0.00	0.00		
R236ea	0.79	0.86	0.93	0.99	1.02	1.02	0.99				
R142b	0.01	0.02	0.02	0.01	0.02	0.01	0.01				
Isobutane	0.32	0.33	0.33	0.31	0.27	0.19	0.07				
R236fa	0.45	0.42	0.35	0.23	0.06						
R124	0.00	0.00	0.00	0.00	0.00						

R318	1.66	1.62	1.37
R1234ze	0.00		
R227ea	0.00		

Table 3. Relative error in approximating the heat input, unit:%

Fluid	Evaporation temperature, °C										
	100	105	110	115	120	125	130	135	140	145	150
Toluene	0.02	0.02	0.02	0.03	0.03	0.03	0.04	0.04	0.05	0.05	0.05
Benzene	0.04	0.04	0.05	0.05	0.06	0.07	0.08	0.09	0.09	0.10	0.11
Cyclohexane	0.04	0.05	0.05	0.06	0.07	0.08	0.08	0.09	0.10	0.11	0.12
Cyclopentane	0.10	0.12	0.13	0.14	0.16	0.18	0.19	0.21	0.23	0.26	0.28
Acetone	0.06	0.07	0.08	0.09	0.10	0.12	0.13	0.15	0.17	0.18	0.20
R113	0.12	0.14	0.15	0.17	0.19	0.21	0.23	0.25	0.28	0.31	0.34
R141b	0.18	0.20	0.22	0.25	0.28	0.31	0.33	0.37	0.40	0.43	0.47
R11	0.22	0.25	0.28	0.31	0.34	0.38	0.42	0.45	0.50	0.55	0.59
pentane	0.18	0.20	0.22	0.24	0.27	0.29	0.32	0.35	0.38	0.41	0.45
Isopentane	0.22	0.25	0.28	0.30	0.33	0.37	0.40	0.43	0.47	0.51	0.56
R123	0.22	0.25	0.28	0.31	0.34	0.38	0.42	0.46	0.50	0.55	0.60
R245ca	0.23	0.26	0.29	0.33	0.36	0.40	0.44	0.48	0.53	0.59	0.64
Cisbutene	0.41	0.46	0.51	0.57	0.62	0.69	0.75	0.83	0.91	0.99	1.09
Transbutene	0.46	0.51	0.56	0.62	0.69	0.76	0.83	0.91	1.00	1.11	1.24
R245fa	0.36	0.40	0.45	0.50	0.55	0.61	0.67	0.73	0.81	0.90	1.01
Butane	0.49	0.55	0.61	0.67	0.73	0.80	0.88	0.97	1.06	1.17	1.32
Butene	0.58	0.64	0.71	0.79	0.87	0.96	1.06	1.17	1.31		
R114	0.50	0.55	0.61	0.68	0.75	0.82	0.91	1.01	1.11		
Isobutene	0.59	0.66	0.73	0.80	0.89	0.98	1.08	1.20	1.34		
R236ea	0.47	0.53	0.59	0.65	0.73	0.80	0.88				
R142b	0.66	0.74	0.82	0.92	1.02	1.13	1.27				
Isobutane	1.52	1.57	1.62	1.67	1.71	1.75	1.78				
R236fa	0.67	0.75	0.85	0.96	1.10						
R124	0.84	0.95	1.07	1.21	1.41						

R318	0.83	0.93	1.05
R1234ze	1.16		
R227ea	1.30		

Table 4. Some properties of the working fluids [52-61]

Fluid	Molecular weight	Critical temperature, °C	Critical pressure, MPa	A	B	C
Toluene	92.1384	319.85	4.10	4.08245	1346.382	-53.508
Benzene	78.1	288.9	4.894	4.72583	1660.652	-1.461
Cyclohexane	84.1595	280.49	4.075	4.13983	1316.554	-35.581
Cyclopentane	70.1329	238.45	4.51	4.00288	1119.208	-42.412
Acetone	58.0791	234.95	4.7	4.42448	1312.253	-32.445
R113	187.376	214.06	3.392	4.02936	1112.856	-44.119
R141b	116.950	204.35	4.194	4.020	1063.376	-40.736
R11	137.368	197.95	4.466	4.01447	1043.303	-36.602
Pentane	72.1488	196.65	3.36	3.9892	1070.617	-40.454
Isopentane	72.1488	187.2	3.378	3.97183	1021.864	-43.231
R123	152.9	183.68	3.6618	4.0222	1034.145	-44.747
R245ca	134.0479	174.42	3.925			
Cisbutene	170.0289	162.6	4.225	3.98744	957.06	-36.504
Transbutene	56.1063	155.46	4.027	4.0436	982.166	-30.775
R245fa	134.0479	154.01	3.651	4.1823	997.2	-48.765
Butane	58.1222	151	3.796	4.70812	1200.475	-13.013
Butene	56.1063	146.35.98	4.02	4.24696	1099.207	-8.256
R114	170.921	145.7	3.393	4.15162	1031.026	-27.911
Isobutene	56.1063	144.94	4.009	3.64709	799.055	-46.615
R236ea	152.0384	139.29	3.502			
R142b	100.495	137.05	4.048	4.007	916.0158	-35.5111
Isobutane	58.1222	134.66	3.629	4.3281	1132.108	0.918
R236fa	152.0384	124.92	3.2	4.255888	1004.490	-35.332

R124	136.476	122.2	3.615			
R318	200.0300	115.23	2.777	4.254	1007.399	-30.205
R1234ze	114.04	109.37	3.6363			
R227ea	170.0289	101.75	2.925			

Table 5. Estimated *a*-value of the working fluids in the evaporation temperature range from 100 °C to 150°C, unit: %

Fluid	Evaporation temperature, °C										
	100	105	110	115	120	125	130	135	140	145	150
Toluene	0.05	0.06	0.07	0.08	0.09	0.10	0.12	0.14	0.15	0.17	0.19
Benzene	0.22	0.24	0.26	0.29	0.31	0.34	0.37	0.40	0.43	0.46	0.50
Cyclohexane	0.27	0.30	0.32	0.35	0.38	0.41	0.45	0.48	0.52	0.56	0.60
Cyclopentane	0.62	0.66	0.71	0.76	0.82	0.88	0.93	1.00	1.05	1.15	1.24
Acetone	0.42	0.46	0.50	0.54	0.59	0.64	0.69	0.74	0.80	0.86	0.92
R113	0.86	0.93	1.00	1.07	1.15	1.23	1.32	1.42	1.52	1.62	1.73
R141b	0.96	1.07	1.18	1.30	1.42	1.55	1.66	1.77	1.89	2.01	2.14
R11	1.35	1.44	1.55	1.65	1.76	1.89	2.04	2.17	2.30	2.45	2.61
Pentane	1.09	1.20	1.29	1.37	1.47	1.56	1.66	1.77	1.88	2.00	2.23
Isopentane	1.55	1.66	1.77	1.89	2.02	2.16	2.30	2.45	2.62	2.79	2.97
R123	1.47	1.57	1.69	1.81	1.94	2.08	2.22	2.37	2.54	2.71	2.89
R245ca	1.59	1.71	1.85	1.99	2.14	2.30	2.47	2.65	2.84	3.05	3.27
Cisbutene	2.63	2.81	2.99	3.19	3.40	3.62	3.85	4.10	4.36	4.65	4.95
Transbutene	2.95	3.14	3.35	3.57	3.81	4.06	4.32	4.61	4.91	5.24	5.61
R245fa	2.38	2.56	2.75	2.96	3.18	3.42	3.67	3.95	4.24	4.56	4.91
Butane	3.28	3.49	3.72	3.97	4.22	4.50	4.79	5.11	5.44	5.81	6.22
Butene	3.72	3.96	4.21	4.49	4.78	5.04	5.42	5.86	6.43	7.40	
R114	3.76	4.00	4.26	4.53	4.83	5.15	5.49	5.86	6.26	6.71	
Isobutene	3.86	4.11	4.38	4.66	4.97	5.29	5.64	6.02	6.44		
R236ea	3.38	3.63	3.90	4.18	4.49	4.83	5.18	5.57			
R142b	4.15	4.43	4.73	5.05	5.40	5.78	6.19	6.65			
Isobutane	4.85	5.17	5.50	5.86	6.25	6.67	7.13				
R236fa	4.73	5.10	5.51	5.96	6.46						

R124	5.54	5.95	6.39	6.87	7.41
RC318	6.31	6.80	7.36		
R1234ze	7.40	8.63			
R227ea	9.07				

Table 6. Estimated efficiency of the working fluids, unit: %

Fluids	Evaporation temperature, °C											
	100		110		120		130		140		150	
	$\eta_{t,EHST}$	$\mu(\eta_t)$	$\eta_{t,EHST}$	$\mu(\eta_t)$	$\eta_{t,EHST}$	$\mu(\eta_t)$	$\eta_{t,EHST}$	$\mu(\eta_t)$	$\eta_{t,EHST}$	$\mu(\eta_t)$	$\eta_{t,EHST}$	$\mu(\eta_t)$
Toluene	10.5	0.07	11.5	0.12	12.4	0.2	13.3	0.29	14.1	0.43	14.8	0.56
Benzene	10.6	0.0	11.6	0.0	12.5	0.0	13.4	0.0	14.1	0.0	14.9	0.0
Cyclo-hexane	10.3	0.4	11.3	0.7	12.2	0.9	13.0	1.2	13.7	1.5	14.4	1.8
Cyclo-pentane	10.3	0.21	11.2	0.26	12.1	0.23	12.9	0.25	13.3	0.27	13.6	0.28
Acetone	10.5	0.0	11.5	0.0	12.4	-0.1	13.2	-0.1	13.9	-0.1	14.6	-0.1
R113	9.9	1.0	10.8	1.2	11.6	1.5	12.3	1.7	13.0	1.9	13.5	2.2
R141b	10.1	0.22	11.0	0.09	11.8	0.05	12.5	0.0	13.1	0.0	13.7	0.0
R11	10.1	0.00	11.0	-0.1	11.7	-0.2	12.4	-0.2	13.1	-0.3	13.6	-0.3
Pentane	9.79	1.74	10.6	1.99	11.3	2.27	12.0	2.62	12.6	2.94	13.1	3.22
Iso-pentane	9.7	1.8	10.5	2.2	11.2	2.6	11.8	2.9	12.4	3.2	12.9	3.4
R123	9.8	0.2	10.6	0.2	11.4	0.2	12.0	0.2	12.6	0.1	13.0	0.0
R245ca	9.6	0.8	10.4	0.9	11.1	1.0	11.6	1.0	12.1	1.0	12.5	0.9
Cis-butene	9.6	-0.3	10.4	-0.4	11.0	-0.4	11.6	-0.5	12.0	-0.6	12.2	-0.5
Trans-butene	9.4	-0.3	10.2	-0.3	10.8	-0.4	11.3	-0.5	11.6	-0.6	11.7	-0.4
R245fa	9.3	0.5	10.1	0.4	10.7	0.4	11.1	0.2	11.5	-0.1	11.5	-0.3
Butane	9.3	0.3	10.0	0.2	10.5	0.1	11.0	-0.1	11.3	-0.3	11.2	-0.4
Butene	9.22	-0.3	9.89	-0.4	10.4	-0.5	10.8	-0.6	10.9	-0.7		
R114	8.98	0.39	9.62	0.35	10.1	0.19	10.5	-0.1	10.6	-0.7		

Isobutene	9.1	-0.3	9.8	-0.4	10.3	-0.6	10.7	-0.7	10.8	-0.4
R236ea	8.9	0.9	9.6	0.9	10.0	0.7	10.4	0.4		
R142b	9.08	-0.2	9.70	-0.3	10.1	-0.2	10.3	0.08		
Isobutane	8.8	-0.1	9.4	-0.3	9.8	-0.5	9.9	-0.6		
R236fa	8.5	0.1	8.9	-0.2	9.0	-0.3				
R124	8.5	-0.6	8.9	-0.5	9.0	0.6				
RC318	7.9	2.4	8.1	1.5						
R1234ze	7.89	-0.1								
R227ea	7.0	-0.6								

Table 7. T_{EHST} of the working fluids with a degree of superheat of 5 °C at the expander inlet, unit: °C

Fluid	Evaporation temperature, °C										
	100	105	110	115	120	125	130	135	140	145	150
Toluene	90.3	93.9	97.5	100.9	104.3	107.6	110.8	114.0	117.1	120.1	123.1
Benzene	90.4	94.0	97.6	101.0	104.4	107.7	110.9	114.0	117.1	120.1	123.1
Cyclohexane	89.1	92.6	95.9	99.2	102.4	105.5	108.6	111.6	114.5	117.3	120.0
Cyclopentane	89.4	92.9	96.2	99.5	102.7	105.8	108.8	111.8	114.7	117.4	120.1
Acetone	90.2	93.8	97.2	100.6	103.9	107.1	110.2	113.2	116.2	119.0	121.8
R113	87.0	90.3	93.4	96.4	99.3	102.2	104.9	107.6	110.1	112.6	115.1
R141b	88.3	91.6	94.8	98.0	101.0	103.9	106.8	109.5	112.1	114.7	117.1
R11	88.6	92.0	95.3	98.4	101.4	104.4	107.2	109.9	112.5	115.0	117.4
Pentane	86.4	89.5	92.6	95.5	98.3	101.1	103.7	106.2	108.7	111.1	113.3
Isopentane	85.9	89.0	92.0	94.8	97.6	100.2	102.8	105.2	107.6	109.9	112.1
R123	86.7	89.9	92.9	95.8	98.6	101.3	103.9	106.4	108.8	111.0	113.2
R245ca	85.5	88.5	91.4	94.1	96.8	99.3	101.7	103.9	106.1	108.1	110.0
Cisbutene	86.6	89.7	92.6	95.4	98.1	100.6	103.0	105.3	107.4	109.3	111.0
Transbutene	86.0	89.0	91.8	94.5	97.1	99.5	101.8	103.9	105.8	107.5	109.0
R245fa	84.7	87.5	90.3	92.8	95.3	97.6	99.7	101.7	103.5	105.1	106.5
Butane	85.0	87.9	90.6	93.2	95.7	98.0	100.2	102.2	104.0	105.6	107.0
Butene	85.3	88.1	90.8	93.4	95.8	98.0	100.1	101.9	103.6	104.9	85.3
R114	83.7	86.4	89.0	91.4	93.7	95.8	97.7	99.5	101.0	102.3	83.7

Isobutene	84.9	87.7	90.4	92.9	95.3	97.4	99.5	101.2	102.8
R236ea	83.0	85.6	88.1	90.4	92.6	94.7	96.6	98.2	
R142b	84.8	87.5	90.1	92.5	94.7	96.7	98.4	99.8	
Isobutane	83.6	86.2	88.7	91.0	93.1	95.1	96.8		
R236fa	81.3	83.6	85.7	87.6	89.2				
R124	82.4	84.8	87.0	88.9	90.5				
R318	79.1	81.2	83.0						
R1234ze	80.6	82.6							
R227ea	77.6								

Table 8. Estimated efficiency of the working fluids with a degree of superheat of 5 ºC at the expander inlet, unit: %

Fluids	Evaporation temperature, ºC											
	100		110		120		130		140		150	
	$\eta_{t,EHST}$	$\mu(\eta_t)$	$\eta_{t,EHST}$	$\mu(\eta_t)$	$\eta_{t,EHST}$	$\mu(\eta_t)$	$\eta_{t,EHST}$	$\mu(\eta_t)$	$\eta_{t,EHST}$	$\mu(\eta_t)$	$\eta_{t,EHST}$	$\mu(\eta_t)$
Toluene	10.6	0.2	11.6	0.3	12.5	0.4	13.4	0.6	14.2	0.7	14.9	0.9
Benzene	10.6	0.0	11.6	0.0	12.5	0.0	13.4	0.0	14.1	0.0	14.9	0.1
Cyclo-hexane	10.4	0.9	11.3	1.2	12.2	1.4	13.0	1.8	13.8	2.1	14.5	2.5
Cyclo-pentane	10.4	0.2	11.3	0.3	12.2	0.4	13.0	0.5	13.7	0.6	14.3	0.7
Acetone	10.5	0.0	11.5	-0.1	12.4	-0.1	13.2	-0.1	13.9	-0.1	14.6	-0.1
R113	10.0	1.7	10.9	1.9	11.7	2.2	12.4	2.5	13.0	2.7	13.6	2.9
R141b	10.1	0.4	11.0	0.3	11.8	0.2	12.6	0.1	13.2	0.1	13.8	0.1
R11	10.1	-0.1	11.0	-0.2	11.8	-0.2	12.6	-0.3	13.2	-0.3	13.7	-0.4
Pentane	9.8	2.6	10.7	3.0	11.5	3.4	12.2	3.8	12.8	4.2	13.3	4.5
Iso-pentane	9.7	2.8	10.5	3.2	11.3	3.6	11.9	4.0	12.5	4.3	13.0	4.6
R123	9.8	0.5	10.7	0.6	11.4	0.6	12.1	0.6	12.7	0.5	13.1	0.5
R245ca	9.6	1.5	10.4	1.6	11.2	1.7	11.8	1.8	12.3	1.8	12.7	1.7
Cis-butene	9.7	-0.2	10.4	-0.3	11.1	-0.4	11.7	-0.5	12.1	-0.7	12.5	-0.8
Trans-butene	9.5	0.0	10.3	-0.1	10.9	-0.2	11.4	-0.4	11.8	-0.6	12.1	-0.9
R245fa	9.4	1.0	10.2	1.0	10.8	1.0	11.3	0.8	11.7	0.6	11.9	0.2
Butane	9.3	0.8	10.0	0.8	10.6	0.7	11.1	0.6	11.5	0.3	11.7	-0.2
Butene	9.3	-0.2	10.0	-0.3	10.6	-0.5	11.0	-0.7	11.2	-1.4		

R114	9.1	1.3	9.7	1.2	10.3	1.1	10.7	0.8	11.0	0.3
Isobutene	9.2	0.0	9.9	-0.2	10.5	-0.4	10.9	-0.7	11.1	-1.0
R236ea	9.0	1.8	9.7	1.8	10.2	1.8	10.6	1.5		
R142b	9.2	-0.4	9.8	-0.6	10.3	-0.7	10.6	-0.8		
Isobutane	8.9	0.5	9.5	0.3	10.0	0.0	10.3	-0.5		
R236fa	8.6	1.0	9.1	0.6	9.4	0.1				
R124	8.6	-0.6	9.1	-0.9	9.4	-1.2				
R318	8.0	4.4	8.4	3.7						
R1234ze	8.1	-1.1								
R227ea	7.4	-0.5								

Table 9. Some properties of HFO1336mzzZ

Parameter	Value	Parameter	value
Critical temperature	171.3 °C	ODP	0
Critical pressure	2.9 MPa	GWP	9
Latent heat at 298.15 K	168.12 kJ/kg	Boiling point	33.4 °C
Safety group (ASHRAE)	A1	Molecular weight	164 g/mol
A, in Antoine Equation	5.786889	M	1961.44, kg/m^3
B, in Antoine Equation	842.20	N	608.99, kg/m^3
C, in Antoine Equation	-83.40493	β	0.32

Table 10. Thermodynamic parameters of HFO1336mzzZ at saturation state [48, 49]

Parameter	Temperature, °C						
	30	100	110	120	130	140	150
$h_{l,s}$, kJ/kg	233.9	325.35	338.73	353.52	369.72	385.21	402.82
$h_{v,s}$, kJ/kg	400.54	454.25	460.60	468.01	474.01	478.41	482.22
$s_{l,s}$, kJ/kg/K	1.13	1.40	1.44	1.48	1.52	1.56	1.60
$s_{v,s}$, kJ/kg/K	1.68	1.75	1.76	1.77	1.78	1.79	1.79
$v_{v,s}$, m^3/kg	6.19	49.3	58.63	82.67	102.33	134.3	179.9
p_s, MPa	0.09	0.72	0.89	1.18	1.42	1.69	2.03

Table 11. Estimated efficiency of HFO1336mmZ compared with R245fa

Parameter		Fluid	Evaporation temperature, °C					
			100	110	120	130	140	150
a-value, %		HFO1336mmZ	1.49	1.73	2.02	2.30	2.64	3.03
		R245fa	2.32	2.67	3.06	3.52	4.09	4.94
T_{EHST}, °C		HFO1336mmZ	83.17	88.23	93.00	97.14	100.93	104.18
		R245fa	84.24	89.64	94.50	98.67	101.95	103.50
$\eta_{t,EHST}$,%	ε_p =0.50	HFO1336mmZ	9.20	9.89	10.49	10.98	11.39	11.70
		R245fa	9.18	9.87	10.43	10.86	11.11	11.06
	ε_p =0.65	HFO1336mmZ	9.31	10.02	10.65	11.17	11.62	11.98
		R245fa	9.35	10.07	10.69	11.17	11.49	11.53
	ε_p =0.80	HFO1336mmZ	9.37	10.10	10.75	11.30	11.77	12.16
		R245fa	9.45	10.20	10.84	11.36	11.73	11.82

Nomenclature

a	ratio of pump power to expander power	EHST	equivalent hot side temperature
$A-C$	coefficients	FOM	Figure of Merit
$A'-E'$			
C	heat capacity, $kJ/kg\cdot K$	GWP	Global Warming Potential
h	enthalpy, kJ/kg	ODP	Ozone Depletion Potential
Hv	vaporization latent heat， kJ/kg	ORC	organic Rankine cycle
Ja	Jacobs number	REFP	REFPROP
M	Coefficient	**Subscripts/ Superscript**	
N	Coefficient	1–4	state points
P	pressure, MPa	bp	boiling point
q	specific heat, kJ/kg	c	critical
S	entropy, $kJ/kg\cdot K$	$cond$	condensation
T	temperature, ^oC	e	expander
v	specific volume, m^3/kg	g	generator
V	volume, m^3	i	input
w	specific work, kJ/kg	id	ideal
Greek Symbols		L	liquid
β	Ising critical exponents	o	output
ε	mechanic efficiency	$over$	overall
η	efficiency	p	pressure/ pump
μ	deviation	r	reference
ρ	density, kg/m^3	s	isentropic/ saturated
τ	Dimensionless temperature	$super$	super heat
Abbreviation		t	thermal
ECST	equivalent cold side temperature	V	vapor